ChemElectroChem

Chemistry Europe
European Chemical Societies Publishing
ChemElectroChem

REVIEW OPEN ACCESS

Biochar-Based Materials for Electrochemical Energy Storage

Valerio C. A. Ficca[1] | Afef Dhaffouli[2] | Rocco Cancelliere[1]

[1]ENEA (Italian National Agency for New Technologies, Energy and Sustainable Economic Development), Department of Energy Technologies and Renewable Sources (TERIN), Division of Technologies and Vectors for Decarbonization (DEC), Laboratory of Technologies and Devices for Electrochemical Storage (ACEL), Casaccia Research Centre, Rome, Italy | [2]Department of chemistry, Faculty of Sciences of Gafsa, University of Gafsa, Laboratory of Interfaces and Advanced Materials, Faculty of Sciences of Monastir, University of Monastir, Monastir, Tunisia

Correspondence: Rocco Cancelliere (rocco.cancelliere@enea.it)

Received: 29 December 2025 | **Revised:** 27 February 2026 | **Accepted:** 23 March 2026

Keywords: battery anodes | biochar | electrochemical energy storage | hard carbon | lithium-ion batteries | potassium-ion batteries | sodium-ion batteries

ABSTRACT

The global transition toward sustainable energy technologies is reshaping the design principles of electrochemical energy storage systems. Biochar, a tunable, carbon-rich material derived from biomass, has emerged as a promising platform for next-generation electrodes due to its abundant feedstock, cheapness, tailored porosity, intrinsic heteroatom content, and renewable origin. In this review, we critically examine recent advances in engineering the physicochemical properties of biochar to enhance its electrochemical performance in batteries. We highlight how microstructural control, surface functionality, and graphitization influence charge storage, ion diffusion, and cycling stability. Emphasis is placed on the interplay between synthesis conditions and electrochemical function, offering insights into structure–property relationships. Finally, we discuss the challenges of standardization, scale-up, and environmental trade-offs, and outline strategies for integrating biochar into scalable, low-carbon energy storage technologies aligned with circular economy principles.

1 | Introduction

Carbon is fundamental to life on Earth. Although it ranks only 15th in abundance in the Earth's crust, its origin from stellar nucleosynthesis and unparalleled bonding versatility give rise to extraordinary chemical diversity, with more known compounds than any other element [1–3]. On our planet, carbon primarily cycles through natural processes; yet modern society increasingly depends on synthetic carbon-based materials [4], including plastics [5, 6], textiles [7], paper [8], wood products [9], and fuels [10]. The extraction, processing, and large-scale deployment of these materials are progressively disrupting environmental equilibria [11].

The historical "take–make–waste" economic model has left a lasting legacy, presenting profound societal and technological challenges, particularly in the context of climate instability and resource insecurity [12]. In response, the European Union (EU) has placed circularity, renewable feedstocks, and sustainable secondary raw materials as central pillars of its long-term strategy, targeting climate neutrality by 2050 [13, 14]. Within this framework, decarbonizing energy systems extends beyond renewable electricity generation: large-scale deployment of intermittent sources such as solar and wind critically depends on scalable, sustainable, and geopolitically secure energy-storage technologies capable of grid stabilization, energy buffering, and electrified mobility [15, 16].

Alkali-metal intercalation batteries, most notably lithium-ion batteries (LIBs), currently dominate electrochemical energy storage (EES) [17–20]. However, their rapid global adoption is increasingly constrained by dependence on critical raw materials (CRMs), including lithium (Li), cobalt (Co), nickel (Ni), and

Valerio C. A. Ficca and Rocco Cancelliere contributed equally to this work.

graphite-based anodes [21–23]. Natural graphite is predominantly fossil-derived, energy-intensive to process, and subject to pronounced supply-chain concentration [24–27]. Recognizing these vulnerabilities, graphite has been formally designated as a CRM in the EU, highlighting the urgency of diversifying carbon architectures for energy storage [28, 29].

In parallel, substantial efforts are being directed toward alternative battery chemistries based on more abundant and geographically distributed elements, particularly sodium and potassium. Sodium-ion batteries (NIBs) and potassium-ion batteries (KIBs) retain the intercalation–deintercalation mechanisms of LIBs while relying on earth-abundant resources, rendering them intrinsically more sustainable and geopolitically resilient [30, 31]. While significant progress has been achieved for cathode materials, the anode remains a critical bottleneck, limiting rate capability, cycling stability, and overall coulombic efficiency.

Among candidate anode materials, carbonaceous structures dominate due to their abundance, chemical stability, and relatively low volume expansion during cycling [32, 33]. Yet, the continued reliance on mined graphite, now strategically at risk, underscores the need for renewable, structurally distinct carbon frameworks capable of supporting next-generation EES systems [34, 35]. In Figure 1, current trends in the anode market and the applications of carbon materials in battery technologies are shown.

Within this context, biochar has emerged as a highly promising alternative. Biochar is a renewable, carbon-rich material produced through the thermochemical conversion of biomass, with its structure readily tunable through pyrolysis temperature (PT) and processing conditions [36, 37]. Low-temperature pyrolysis (<900°C) yields highly functionalized, amorphous carbons rich in oxygen-containing groups, whereas higher temperature treatment (typically > 900°C) produces hard carbons (HCs), a nongraphitizable yet structurally robust phase characterized by turbostratic short-range order, enlarged interlayer spacing, and closed nanopores [38–41].

Unlike petroleum-derived carbons, which can undergo graphitization at extreme temperatures, biomass-derived carbons remain intrinsically nongraphitizable due to their molecular heterogeneity and cross-linked aromatic structure [42–45]. This intrinsic disorder is advantageous for alkali-ion storage, particularly in NIBs, where enlarged interlayer spacing and disordered pore networks enable ion-storage mechanisms inaccessible to crystalline graphite [46, 47].

Beyond structural tunability, biochar can be produced from a wide range of renewable feedstocks [48], including agricultural residues, forestry by-products, food-processing waste, and marine biomass. Scalable synthesis routes such as slow pyrolysis, hydrothermal carbonization, molten-salt processing, and physical or chemical activation [49–53] allow precise control over porosity, surface chemistry, defect density, interlayer spacing, and heteroatom incorporation, within the limits of nongraphitizable carbon frameworks [48]. As a result, biochar-based carbons have emerged as environmentally friendly and functionally competitive alternatives to commercial graphite across multiple electrochemical systems [54, 55].

In EES, biomass-derived HCs have demonstrated significant potential not only for LIBs and NIBs but also for emerging technologies such as KIB, lithium–sulfur batteries (Li–S), dual-ion capacitors, and metal–air systems [56–58]. Their disordered microstructure supports a combination of surface adsorption, interlayer intercalation, and low-voltage pore-filling mechanisms, while heteroatom doping and defects engineering further enhance electronic conductivity and interfacial kinetics [59–61]. Increasingly, well-engineered biochar-based electrodes achieve high reversible capacity, strong rate performance, and long cycle life while enabling decentralized, low-carbon production pathways consistent with circular-economy principles [56, 59].

Despite this progress, substantial challenges remain. Biomass feedstocks are intrinsically heterogeneous, with variations in ash content, lignocellulosic composition, and metal impurities, all of which influence carbon yield, microtexture, and electrochemical behavior [62]. Even under controlled synthesis conditions, batch-to-batch reproducibility remains a major barrier to industrial deployment [63]. Moreover, aggressive activation strategies and high-temperature treatments, while effective in boosting performance, can compromise environmental sustainability, scalability, and safety, necessitating careful life-cycle and techno-economic evaluations [64, 65].

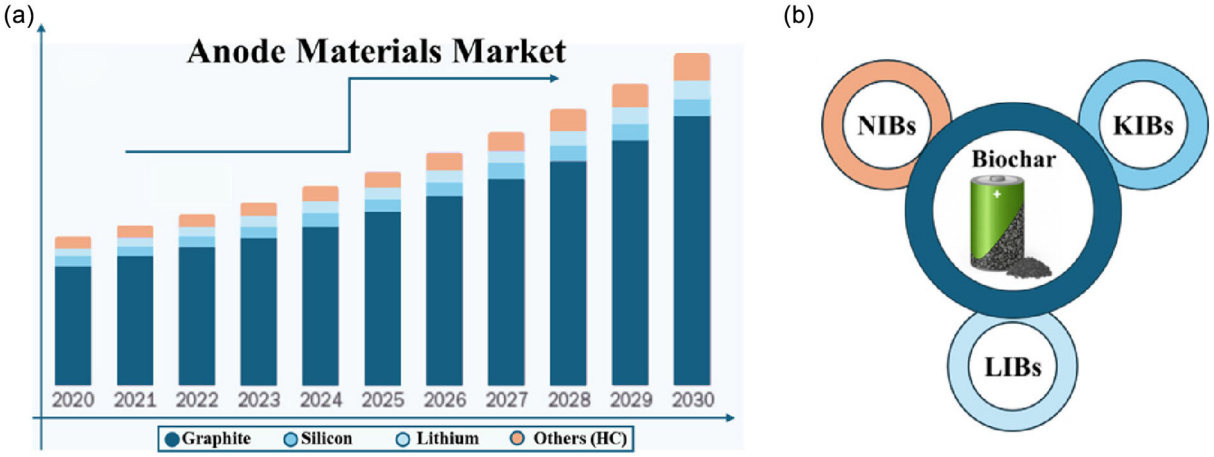

FIGURE 1 | Current trends and applications of carbon materials in battery technologies. (a) Global anode materials market landscape. (b) Main applications of nongraphitic carbons in intercalation-type batteries, including LIBs, NIBs, and KIBs.

In the last 2 years, several recent reviews published in the literature have comprehensively examined biomass-derived carbons for electrochemical applications, with particular emphasis on sodium-ion storage mechanisms, heteroatom-doping strategies, and high-surface-area architectures for enhanced capacity [66–69]. These studies have significantly advanced understanding of defect-mediated sodium storage and pore-filling mechanisms in HCs, frequently highlighting record capacities achieved through microstructural engineering and surface functionalization [33, 70–72]. Complementary analyses have addressed sustainability metrics and life-cycle considerations of biomass-derived electrodes, underscoring the role of feedstock circularity and environmental impact in carbon-material development.

Notwithstanding these advances, a unifying comparative framework across LIBs, NIBs, and KIBs remains insufficiently articulated. Existing reviews commonly treat these chemistries independently and rarely establish systematic correlations between ionic radius, carbon microstructure, defect chemistry, and the governing ion-storage mechanisms. Likewise, the interplay between graphite-substitution strategies in LIBs, HC optimization for NIBs, and defect-rich architectures for KIBs has not been critically synthesized within a single integrative perspective. As a result, materials design principles are often presented in isolation rather than positioned along an ion-dependent structural continuum.

The present review addresses this gap by establishing cross-system correlations and defining ion-specific materials-design gradients for biochar-derived carbons. Moving beyond capacity-driven reporting, we adopt a mechanism-informed framework that links pyrolysis chemistry, microstructural evolution, heteroatom functionality, and pore architecture to alkali-ion storage behavior. Specifically, we critically analyze how synthesis strategies, activation pathways, and feedstock variability shape structure–property relationships; examine approaches to mitigate batch-to-batch heterogeneity; and outline scalable routes for integrating biochar-based carbons into low-carbon, geopolitically resilient energy-storage architectures aligned with circular-economy objectives.

2 | Classification of Carbon Materials: From Soft to HC

Carbon materials are commonly classified according to their degree of structural order and their ability to undergo graphitization upon high-temperature treatment [73]. Ordered carbons, exemplified by graphite, exhibit long-range stacking of sp^2 graphene layers with well-defined crystallographic coherence and an interlayer spacing (d_{002}) of ≈0.335 nm [74–77]. In contrast, disordered carbons consist of turbostratic, misaligned graphene domains characterized by limited stacking order, rotational disorder, and enlarged interlayer spacing. Beyond structural order, a more fundamental distinction is provided by graphitizability. Graphitizable carbons, often referred to as soft carbons, can reorganize into crystalline graphite above ∼2500°C–2800°C through thermally activated layer realignment. Nongraphitizable carbons, by contrast, retain a rigid, cross-linked aromatic framework even under extreme heat treatment, as their microstructure kinetically inhibits graphitic ordering [74, 75, 78].

Within this framework, biowaste-derived carbons occupy a distinctive and nonoverlapping domain. Their heteroatom-rich composition, molecular irregularity, and intrinsically cross-linked aromatic architecture inhibit true graphitization, even at temperatures exceeding those required for petroleum-derived precursors [79]. Unlike pitch, coke, or carbon black, classified as graphitizable soft carbons, biomass-derived carbons are inherently nongraphitizable [43, 80]. Their thermal evolution therefore proceeds along a continuous pathway from low-temperature biochar to high-temperature HCs, both residing within Kinoshita's nongraphitizing carbon framework (see Figure 2) [75]. This distinction underpins their unique morphological, electronic, and electrochemical behavior in energy-storage systems.

At low PTs (typically 300°C–500°C), biomass decomposition is incomplete, yielding a material commonly referred to as Low-T biochar [81, 82]. This early-stage carbon is structurally heterogeneous and chemically rich, containing abundant oxygenated surface groups (e.g., carboxyl, hydroxyl, carbonyl functionalities), residual lignocellulosic motifs, small aromatic clusters, and low fixed-carbon content [75, 83]. Although sometimes described as

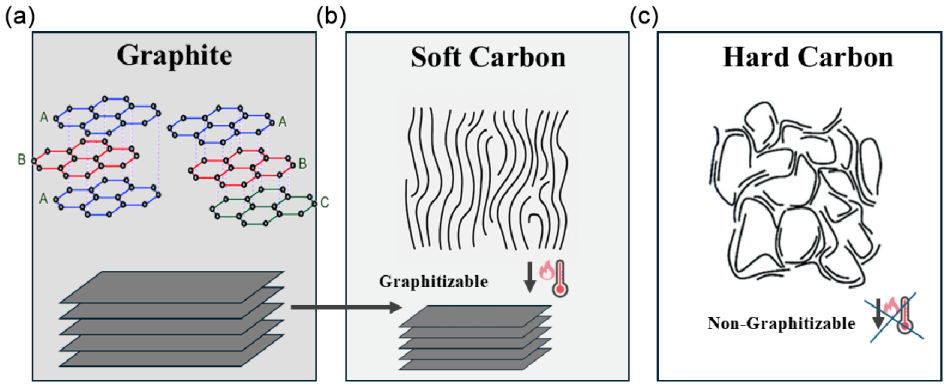

FIGURE 2 | Structural hierarchy and graphitizability of carbon materials. Schematic comparison of (a) graphite, (b) graphitizable soft carbons, and (c) nongraphitizable HC, illustrating the progressive loss of stacking order and increasing topological constraint from ordered graphite to disordered biomass-derived carbons. Graphite exhibits long-range AB-stacked graphene layers with well-defined interlayer spacing. Soft carbons consist of turbostratic graphene domains that retain sufficient structural mobility to reorganize into crystalline graphite upon high-temperature treatment (>2500°C–2800°C). In contrast, HCs are composed of highly curved, cross-linked aromatic fragments forming rigid three-dimensional networks with closed porosity, which kinetically inhibit graphitic ordering even under extreme thermal conditions. Adapted from [75].

"soft-carbon-like" in terms of disorder, such materials are not graphitizable soft carbons in the strict structural sense, as they lack the mesophase-forming intermediates required for graphitic reorganization. Their high polarity, wettability, and surface reactivity may be advantageous for catalysis, capacitive storage, or sensing applications, but they severely limit battery performance [36, 83, 84]. In this regime, biochar exhibits low electronic conductivity, high irreversible capacity loss, unstable solid–electrolyte interphase (SEI) formation, and sluggish charge-transfer kinetics, precluding efficient and reversible alkali-ion intercalation [38, 85].

Increasing the PT to intermediate values (~600–900°C) drives dehydration, deoxygenation, aromatization, and polycondensation reactions, progressively transforming biochar into a more carbon-rich and structurally coherent material [86]. Turbostratic nanodomains emerge, heteroatom content decreases, and hierarchical porosity develops as cellulose- and hemicellulose-derived microstructures collapse. These transformations are typically accompanied by a decrease in interlayer spacing toward ~0.36–0.38 nm, a reduction in Raman I_D/I_G ratio dispersion, and a marked increase in electronic conductivity [60, 87]. In this transitional regime, the material begins to exhibit characteristics associated with HC precursors, including improved SEI stability and the onset of Na^+ insertion. However, electrochemical performance remains strongly dependent on precursor chemistry and residual surface functionality.

True HC is obtained only after high-temperature pyrolysis, typically above 1000°C [88]. In this regime, biomass-derived carbons undergo extensive aromatization and microtexture reorganization, forming highly disordered turbostratic layers composed of curved, misaligned graphene fragments with enlarged interlayer spacing (~0.36 nm) [89]. Crucially, despite this increased short-range ordering, biogenic carbons remain nongraphitizable and do not develop three-dimensional graphitic stacking (AB stacking) [90, 91]. Instead, their structure stabilizes into the characteristic house-of-cards architecture of HC, featuring slit-shaped voids, closed nanopores, and sp^2-rich domains interconnected by topological defects (Figure 2) [92, 93]. These structural motifs enable the three canonical storage mechanisms observed in high-performance NIB anodes: surface adsorption, interlayer intercalation, and low-voltage pore filling. Concurrently, the reduction of surface oxygen groups enhances SEI stability and suppresses parasitic reactions, while increased conductivity supports high-rate operation [94]. In Table 1, a summary and interplay of PT and structural properties is reported.

Electrochemical performance across the pyrolysis spectrum arises from the coupled evolution of carbon microstructure, heteroatom chemistry, and surface energetics [80]. While PT is the primary driver of structural ordering and aromatic condensation, feedstock chemistry establishes the initial boundary conditions for carbon evolution [95]. Lignin-rich precursors (e.g., hardwoods, softwoods, nutshells) yield a higher fixed-carbon content and more condensed aromatic domains upon pyrolysis, producing biochars with lower surface area, reduced oxygen content, and enhanced electronic conductivity [96]. These characteristics favor improved initial Coulombic efficiency (ICE) and enhanced charge transport in LIB systems, where excessive surface functionality promotes irreversible lithium consumption and unstable SEI formation.

In contrast, cellulose- and hemicellulose-rich herbaceous residues undergo rapid devolatilization, generating greater microporosity and higher densities of oxygen-containing functional groups [97]. The resulting defect-rich carbons exhibit lower intrinsic conductivity but possess abundant adsorption sites and enlarged interlayer spacing [98]. While such architectures are less suited for graphite-mimetic LIB performance, they become advantageous in NIB and KIB systems, where defect-mediated adsorption and pore filling dominate the storage mechanism. Mineral constituents naturally present in agricultural biomass (e.g., K, Ca, and Mg) may further catalyze pore development or induce local structural rearrangements during pyrolysis, thereby modulating ion transport pathways and electron transport.

Structural ordering governs conductivity and ion diffusion; high-temperature treatment modulates heteroatom content, electronic structure, redox activity, surface area, defect density, and pore

TABLE 1 | Pyrolysis-temperature-driven structural evolution of biomass and fossil-derived carbons. Typical ranges of PT, feedstock origin, Raman disorder ratio (I_D/I_G), and interlayer spacing (d_{002}) for biochar, HC, soft carbon, and graphite, highlighting the transition from nongraphitizable biomass-derived carbons to graphitizable fossil-based carbon frameworks.

Carbon class	Pyrolysis temperature, °C	Typical feedstock	Raman (I_D/I_G)	d(002), nm	Structural features
Low-T biochar	300–500	Lignocellulosic biomass (straw, shells)	0.7–1.0	0.38–0.42	Amorphous carbon, High O-content Low aromatic clusters
Transitional biochar	600–800	Agricultural waste, lignin-rich residues	0.9–1.2	0.36–0.39	Emerging turbostratic domains, hierarchical porosity
HC	>900	Hardwood, nutshells, biomass chars	1.0–1.4	0.36–0.38	Turbostratic graphene, closed nanopores, nongraphitizable
Soft carbon	>1000 (graphitization >2500)	Pitch, coke, carbon black	0.8–1.1	0.335 after HTT	Graphitizable turbostratic layers
Graphite	>2800 (or natural)	Synthetic,fossil-derived / natural	<0.3	0.335	Long-range AB stacking

Abbreviation: HTT, high-temperature treatment.

architecture, which control interfacial charge-transfer kinetics [99]. Accordingly, low-temperature biochars exhibit high surface reactivity, but limited reversibility, transitional carbons balance conductivity and accessibility, and high-temperature HC optimize ion storage through their turbostratic framework and stabilized surface chemistry [100, 101]. Crucially, regardless of treatment temperature, biomass-derived carbons remain nongraphitizable. This intrinsic topological constraint preserves enlarged interlayer spacing and closed porosity, features essential for efficient Na^+ and K^+ storage [102, 103].

From a materials-design perspective, PT represents the dominant control parameter governing morphology and electrochemical behavior. In contrast, feedstock composition and activation chemistry define the inherent conductivity–functionality–porosity trade-off that thermal treatment subsequently refines. Lignin-rich precursors (e.g., woody biomass) typically yield more condensed aromatic frameworks with lower oxygen content and improved electronic conductivity, thereby favoring higher ICE and stable cycling in LIBs. Conversely, cellulose- and hemicellulose-rich residues generate more disordered carbons with higher microporosity and surface functionality. While such defect-rich structures can enhance Na^+ and K^+ storage through adsorption-dominated mechanisms, they often increase irreversible capacity and reduce ICE due to amplified surface reactivity (cation caging effect). In addition, mineral species (e.g., K, Ca, and Mg) further influence carbon evolution by catalyzing pore formation or local graphitization; however, residual ash may destabilize the SEI and promote parasitic reactions. As a result, applying identical pyrolysis conditions to chemically distinct biomasses can produce markedly different microstructures and electrochemical behaviors, complicating reproducibility and scale-up. Systematic precursor classification, targeted pretreatments (e.g., demineralization), and predictive process–structure–performance models are therefore essential to achieve scalable biochar-based anodes. Resolving this multidimensional optimization remains the central challenge for translating biomass-derived HC into reliable next-generation energy-storage technologies [104, 105].

3 | Biochar-Based Carbons in Alkali Metal-Ion Batteries

Alkali metal-ion batteries, including lithium-, sodium-, and potassium-ion systems, share a common electrochemical foundation: the intercalation-based "rocking-chair" mechanism, first articulated by Scrosati and co-workers, in which alkali ions reversibly shuttle between two host structures during charge and discharge. In Figure 3, a schematic representation of an LIB intercalation battery is reported.

Within this paradigm, the anode plays a central role in governing energy density, rate capability, efficiency, and cycle life, as it must accommodate repeated ion insertion and extraction while maintaining structural and interfacial stability. Carbonaceous materials have therefore emerged as the universal anode platform across alkali-ion chemistries (Li^+ / Na^+ / K^+), owing to their chemical robustness, low volumetric strain, and compatibility with intercalation-based storage.

The rapid scale-up of alkali metal-ion batteries is, however, increasingly constrained by the reliance on graphite and fossil-derived carbons, which are inherently unsustainable. These challenges are amplified as battery technologies expand beyond lithium to sodium and potassium, where the larger ionic radii of Na^+ and K^+ fundamentally limit the applicability of crystalline graphite. This convergence of electrochemical and geopolitical pressures has stimulated intense interest in biomass-derived carbons, particularly biochar and biochar-derived

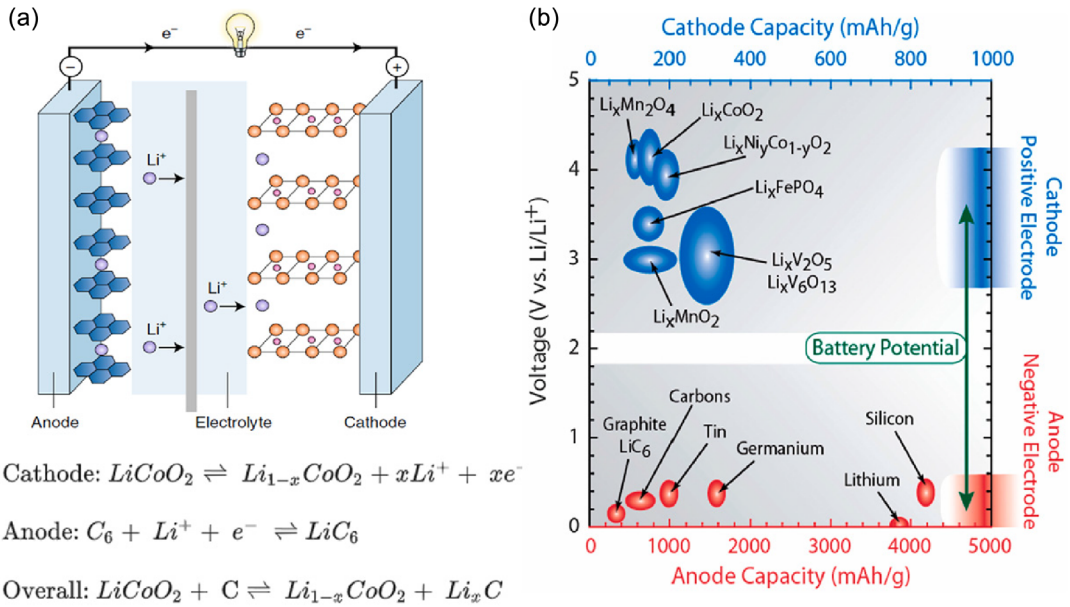

FIGURE 3 | Intercalation-based alkali metal-ion batteries and the central role of carbon anodes. (a) Schematic of a rocking-chair intercalation battery, illustrating reversible alkali-ion shuttling between host electrodes during cycling. (b) Typical specific capacity of carbon anodes in LIBs, highlighting the intrinsic capacity limitation of crystalline graphite and motivating the development of structurally distinct carbon architectures, including biochar-derived HC, for Li-, Na-, and K-ion systems.

HC, as renewable and structurally adaptable alternatives for negative electrodes.

From a materials perspective, most biowaste-derived carbons fall within the HC family already depicted. By tuning synthesis parameters, these materials can access a continuum of storage behaviors, ranging from predominantly intercalation-driven mechanisms to defect-mediated adsorption and pore-filling processes. Although the development of HC has historically been driven by NIBs, the same structural toolbox is increasingly being applied across lithium- and potassium-ion systems, positioning biochar-based carbons as a chemistry-agnostic anode platform.

Beyond electrochemical performance, biowaste-derived carbons offer intrinsic advantages over petroleum cokes and mined graphite. The diversity and abundance of biomass feedstocks enable decentralized production and texture tailoring, while inherent heteroatom content often enables in situ N/O/S doping without additional synthetic steps. When locally sourced and integrated into existing thermal or biorefinery infrastructures, biochar production can achieve competitive life-cycle metrics in terms of energy demand and carbon footprint. At the same time, persistent challenges—most notably low ICE, feedstock variability, and the environmental cost of aggressive activation or graphitization treatments, must be critically addressed to enable industrial deployment.

Against this backdrop, LIBs provide a stringent yet strategically important benchmark for assessing the viability of biochar-based carbons. In Section 3.1, we examine their role in LIBs, both as active anode materials and as conductive or structural components. Sections 3.2 and 3.3 then extend the discussion to NIBs and KIBs, respectively, where HC is already approaching commercial relevance and where the intrinsic structural features of biochar-derived carbons are often better matched to ion size and voltage window than in conventional LIB chemistries.

3.1 | LIBs

In LIBs, biowaste-derived carbons have been deployed in three main roles: (i) as direct alternatives to graphite in the form of biochar or bio-HC anodes; (ii) as engineered "bio-graphites" obtained through catalytic graphitization of biomass-derived precursors; and (iii) as functional additives partially replacing carbon black or other conductive carbons in conventional composite electrodes. Over the past 3 years, the field has evolved from predominantly phenomenological half-cell demonstrations toward more deliberate microstructural design, increasingly coupled with explicit considerations of sustainability, feedstock origin, and circular-economy metrics. A comparative summary of synthesis conditions (including PT), reversible capacity, ICE, and rate performance in recent LIB studies is provided in Table 2 to enable direct comparison across systems.

Attention has been devoted to engineering biochar and bio-HCs as structural alternatives to graphite, aiming to replicate intercalation-dominated lithium storage while maintaining sustainability advantages [125]. In contrast to highly porous carbons that rely predominantly on surface-driven mechanisms, graphite-replacement strategies typically employ controlled pyrolysis (800°C–1200°C) to reduce surface area, suppress excessive defect density, and promote turbostratic microdomains capable of hosting lithium through quasi-intercalation processes [126, 127]. These materials generally deliver reversible capacities in the range of 250–380 mAh g^{-1}, approaching that of graphite, with improved cycling stability but still lower initial coulombic efficiencies due to residual surface functionality and irreversible lithium trapping [128]. Efforts to enhance practical viability have therefore focused on heteroatom regulation, pore closure strategies, prelithiation approaches, and densification treatments to improve volumetric energy density [129]. While complete parity with commercial graphite remains challenging, particularly in terms of ICE and tap density, the literature demonstrates that appropriately engineered bio-HCs can operate within the performance window required for graphite substitution in half-cell configurations [130].

Biomass-derived biochars have attracted significant attention as LIB anode materials owing to their tunable porosity, surface chemistry, and intrinsic heteroatom content. A recurring observation across studies is the strong dependence of electrochemical performance on the biomass precursor and processing conditions. For example, Wang et al. [106] reported nitrogen-doped porous carbons derived from chlorella and oyster shell that exhibited pseudographitic features and delivered a reversible capacity of 1384.9 mAh g^{-1} over 150 cycles at 0.1 A g^{-1}, retaining 737.6 mAh g^{-1} after 1000 cycles at 1.0 A g^{-1}. In a different approach, Ge et al. [107] demonstrated that pine-needle-derived biochar with a hierarchical porous architecture could function both as a conductive additive and as a high-rate anode, providing a stable capacity of 192.3 mAh g^{-1} at 0.5 C. Similarly, Shi et al. [108] showed that biochar obtained from *Poria cocos* waste achieved an exceptionally high surface area (2290.6 m^2 g^{-1}), enabling an initial capacity of 1139.6 mAh g^{-1} at 0.1 A g^{-1} and retaining 806.6 mAh g^{-1} after 300 cycles.

These results illustrate the considerable versatility of biomass-derived carbons in LIBs, but they also highlight a critical limitation: exceptionally high capacities are often dominated by surface-driven storage processes, including adsorption, pseudocapacitive contributions, and extensive SEI formation. Consequently, low ICE and limited volumetric energy density remain persistent challenges for the direct replacement of graphite in practical LIB anodes.

The role of PT in governing lithium storage behavior is well illustrated by bamboo-derived biochars produced via slow pyrolysis. Barbosa et al. [109] reported that biochar synthesized at 800°C delivered a reversible capacity of approximately 230 mAh g^{-1} at a C/5 rate (corresponding to a full charge/discharge in 5 h), whereas increasing the PT to 1000°C resulted in superior high-rate performance, maintaining ~95 mAh g^{-1} at 10 C.

This behavior was attributed to enhanced electronic conductivity and a more open pore network in the high-temperature sample, facilitating faster lithium-ion (Li^+) transport. Electrochemical signatures, including sloping voltage profiles and cyclic voltammetry responses, indicate a hybrid storage mechanism combining surface adsorption with limited intercalation into turbostratic domains, rather than classical graphite-like staging. Notably, both materials exhibited excellent cycling stability, retaining nearly their full capacity after 450 cycles at C/5 (C-rate; see Figure 4).

Beyond their use as standalone anodes, biomass-derived carbons have shown increasing promise as functional additives in LIB. Belmesov et al. [124] reported that prelithiated yellow-pine biochar containing 3 wt% LiF formed microporous soft-carbon-like

TABLE 2 | Summary of the most relevant biochar-derived carbon used as LIB electrode material (2023–2025).

Feedstock	Treatment	Pyrolysis temp., °C	Role in cell	Reversible capacity, mAh g^{-1}	ICE, %	Cycling / Rate performance	Ref.
Chlorella + oyster shell	Ball milling, high-temperature carbonization	n.d.	LIB anode	1385 (@0.1 A/g, 150 cycles); 738 (@1 A/g, 1000 cycles)	n.d.	Stable over 1000 cycles	[106]
Pine needles	Activation (KCl) + thermal treatment + N-doping	n.d.	Conductive additive	192.3 (@0.5 C)	n.d.	Excellent retention	[107]
Poria cocos waste	Chemical–thermal treatment	n.d.	LIB anode	1139.6 (@0.1 A/g); 806.6 (@300 cycles); 227.85 (@1 A/g)	n.d.	Good rate performance	[108]
Bamboo	Slow pyrolysis (B800/B1000)	800 / 1000	LIB anode	250 (@C/5)	n.d.	Stable 450 cycles	[109]
Yellow pine biochar	Carbonization + 3 wt% LiF	1000–1400	LIB anode	256→235	n.d.	$R = 6.6\ \Omega$, $b = 0.75$	[110]
Tannin	CO_2 activation	900	LIB anode	n.d.	n.d.	High SSA 1370 m^2/g; hierarchical porosity	[111]
Antibiotic bacteria residues	Carbonization + incorporation of N and O elements	n.d.	LIB anode	n.d.	n.d.	Layered porous; N-doped; good cycling	[112]
Rice straw	Pyrolysis + activation	n.d.	LIB anode	n.d.	n.d.	Low-cost; good rate	[113]
Market biochar + catalytic treatment	Hybrid catalyst + catalytic Graphitization	n.d.	LIB anode	n.d.	n.d.	Scalable graphitization; improved anode performance	[114]
Discarded bamboo chopsticks	Carbonization + SnO_2 nanosheets	n.d.	LIB anode	1182.5 (initial); 570.5 (500 cycles)	n.d.	500 cycles	[115]
Jack wood	NaOH activation	800	Anode/activated carbon	n.d.	n.d.	High SSA; promotes Li^+ transport	[116]
Olive pomace	H_3PO_4 activation	500	LIB anode	n.d.	n.d.	Eco-friendly precursor; low SSA 10.6 m^2/g	[117]
Cu/MnO-biochar	Metal-oxide functionalization	n.d.	LIB anode	1070 (@0.1 A/g)	100	200 cycles	[118, 119]
Seaweed-derived biochar (Si@N-Gam-5)	N-doping + Si integration	n.d.	LIB anode	1483 (@0.1 A/g)	63.3	n.d.	[120]
Bio-graphite	Biochar graphitization	n.d.	LIB anode	293 (@0.02 A/g)	75.6	n.d.	[114]
Biochar (Rice straw) + spent LIBs	Oxalic acid + microwave activation	n.d.	Microwave catalyst	n.d.	n.d.	Max heating 720°C/min; H_2-rich syngas 50.2 vol%	[121]
Rice husk	Fast pyrolysis	700–800	SiOx/C anode	1366/800/275 (@1st/5th/200th cycles)	n.d.	Conductive pathways; buffers expansion	[122]
Corn stalk	NaOH activation	800	LIB anode	n.d.	n.d.	Improved Li storage; SSA 255 m^2/g	[123]
Red seaweed and seagrass	Stepwise pyrolysis	500–700	LIB anode	391→300		70 % C, >5 % N	[124]

Abbreviations: B800/B1000, bamboo pyrolyzed at 800°C or 1000°C; C, C-rate; ICE, initial Coulombic efficiency; LiF, lithium fluoride; n.d. not determined; SSA, specific surface area; SiOx/C, silicon oxide/carbon composite.

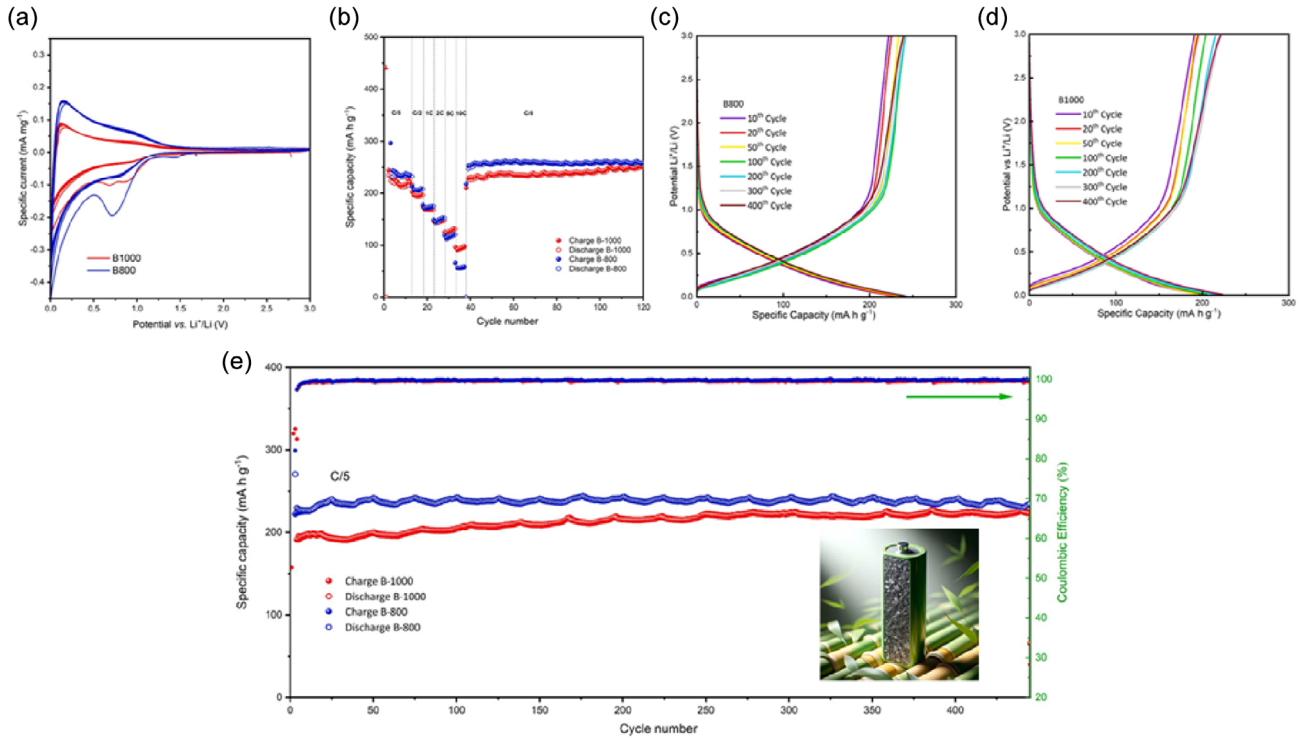

FIGURE 4 | Electrochemical performance of bamboo-derived biochar anodes in LIBs: (a) CV curves at a scan rate of 0.05 mV s^{-1}; (b) rate capability from C/5 to 10 C and back to C/5; (c,d) galvanostatic charge–discharge profiles at C/5; and (e) long-term cycling performance over 450 cycles at C/5. Reproduced from ref. [109]. Creative Commons CC-BY license.

structures that facilitated Li^+ transport, achieving a reversible capacity of 235.25 mAh g^{-1} at 20 mA g^{-1} with low series resistance. Detailed electrochemical analysis, including galvanostatic charge–discharge profiles, Coulombic efficiency (CE), and rate-capability measurements, demonstrated stable performance across a range of operating conditions, underscoring the value of biochar-based carbons as multifunctional components rather than simple conductive fillers (see Figure 5).

Taken together, these examples demonstrate that the electrochemical performance of biochar-based materials in LIBs, including specific capacity, rate capability, and cycling stability, is strongly governed by feedstock selection, PT, and surface functionalization. Controlled processing enables the development of cost-effective and environmentally benign carbons with competitive performance in LIB half-cells. Nevertheless, LIBs remain a stringent benchmark for biomass-derived carbons: the small ionic radius of Li^+, narrow operating voltage window, and strict requirements on ICE strongly favor crystalline graphite. Consequently, while biochar-derived carbons are unlikely to fully displace graphite as LIB anodes in the near term, they represent a compelling platform for conductive additives, hybrid electrode architectures, and mechanistic insight. These findings directly inform their more natural and technologically impactful deployment in NIBs and KIBs, as discussed in Sections 3.2 and 3.3.

3.2 | NIBs

NIBs are emerging as a compelling complement to lithium-ion technology, particularly for stationary storage and cost-sensitive markets, driven by the abundance and broad geographic distribution of sodium (Na) resources, as well as the potential to leverage existing battery manufacturing infrastructure. From an anode perspective, however, NIBs face fundamental limitations with conventional graphite: unlike Li^+, Na^+ does not form a thermodynamically stable intercalation compound in pristine graphitic lattices, rendering graphite largely inactive [131, 132]. Consequently, the anode design space in NIBs is dominated by nongraphitizable disordered carbons (i.e., HC), which enable Na storage through multiple mechanisms, including adsorption at defects/edges, insertion between turbostratic graphene layers, and clustering within porosity and defects of HC [93, 133–136].

The sodium-storage signature of HC is typically decomposed into two voltage regimes: a slope region (>0.1 V) governed primarily by adsorption at defects/edges and shallow insertion into disordered domains, and a low-voltage plateau (<0.1 V), associated with interlayer insertion and pore filling (often described as Na clustering in closed micropores). This mechanistic framework places biochar-derived HC in a privileged position: their microtexture naturally combines turbostratic graphene domains (expanded d_{002}), abundant defect chemistry, and controllable open/closed porosity. Importantly, more interlayer spacing is not always better. Once d_{002} exceeds the minimum required to accommodate Na^+ insertion (often discussed around ~0.37 nm), further expansion does not guarantee higher capacity and may instead correlate with excessive disorder, high surface area, and parasitic reactions [137, 138]. Similarly, oxygen and other heteroatom functionalities are a double-edged sword: carbonyl-rich motifs (e.g., quinone/anhydride-like C = O environments) can provide reversible Na-binding sites and enhance electrolyte wettability, whereas highly labile C═O species increase irreversible capacity via extensive SEI formation. Therefore, NIB anode

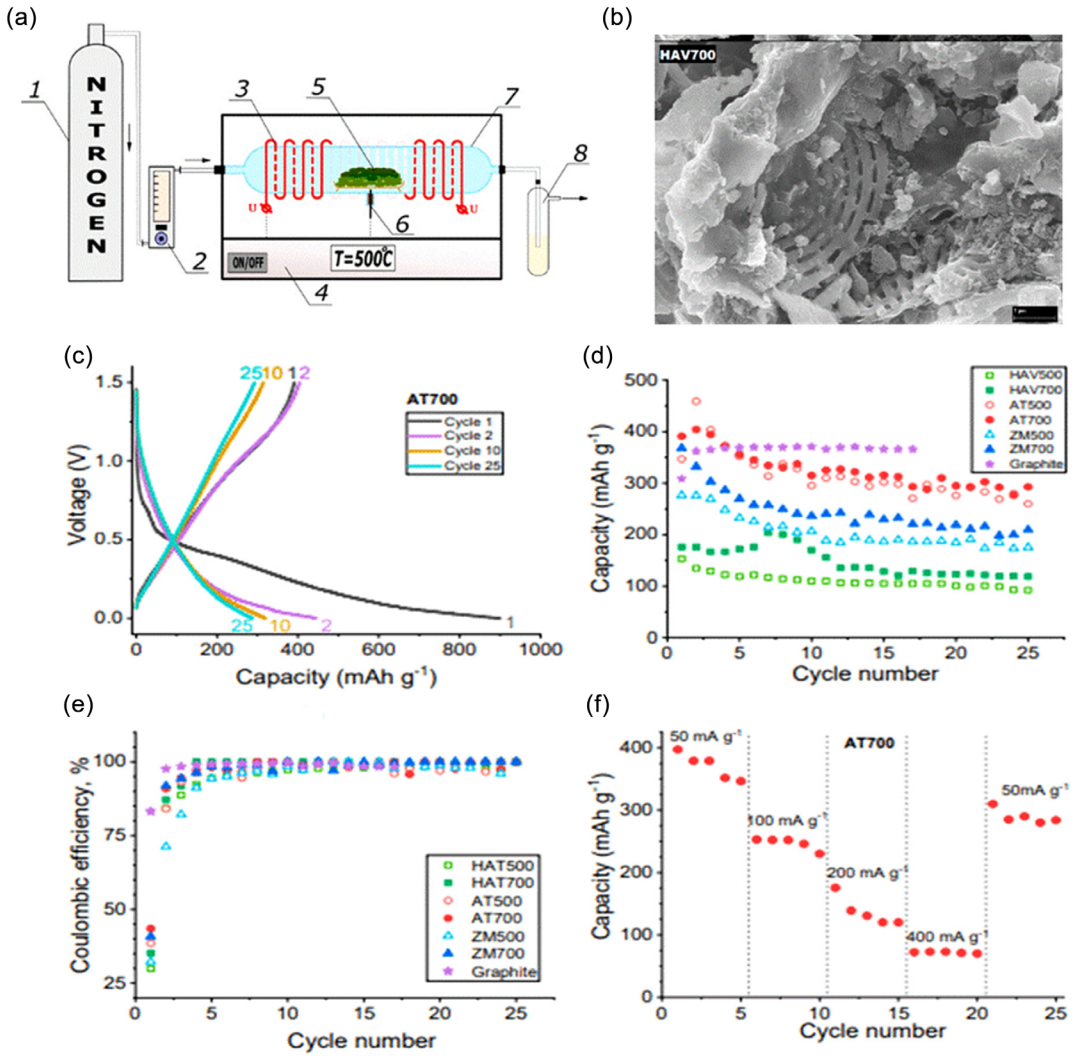

FIGURE 5 | (a) Schematic illustration of biochar synthesis through pyrolysis; (b) representative SEM micrographs of the resulting biochar; (c) galvanostatic charge–discharge profiles of the AT700-based cell; (d) cycling stability of cells employing the investigated biochars; (e) CE measured at a current density of 36 mA g^{-1}; and (f) rate-dependent cycling performance of the AT700 electrode under various charge–discharge conditions. Reproduced from ref. [124], Creative Commons CC-BY license.

optimization is best treated as a multiparameter problem, where capacity, plateau fraction, ICE, and rate capability are jointly dictated by a coupled set of descriptors: d_{002}, closed-pore fraction, active surface area, defect density, and functional-group speciation [139]. Figure 6 summarizes the main understood pathways and mechanisms for Na^+ intercalation in HC.

Across biomass-derived systems, PT remains the first-order tuning of Na-storage behavior because it controls graphitization degree, interlayer spacing, defect density, and pore structure. From the reviewed literature, specific structure–property trends can be highlighted. For low temperatures pyrolysis (700–900°C), the precursors undergo an incomplete carbonization, retaining original biomass features with many defects and oxygen groups. Low PTs are also predominantly associated with a large surface area and modest graphitic ordering. Such features favor high surface capacity but low ICE, corresponding to poorer cycling capabilities due to excessive SEI formation and unstable surface [57, 142–144].

Increasing the PT to the range 1000–1300°C is often considered an optimal window for biomass-derived NIB anodes. At this temperature, the carbonization modifies the microstructure, leading to an appropriate balance between disorder and graphitization, defect content, and expanded interlayer spacing (typically 0.36–0.39 nm). In addition, the formation of useful micro/mesopores is observed. For example, Wu et al. [142] increased the PT from 900°C to 1100°C to prepare pomegranate peel-derived HC (PPHC-1100), obtaining an interlayer spacing ~0.38 nm, a suitable oxygen content, and low surface area (1.7 m^2 g^{-1}), delivering 330 and 175 mAh g^{-1} after 200 cycles. Also, olive-pomace HC shows strong enhancement when increasing PT from 750 to 1250°C, increasing the specific capacity from 94 to 248 mAh g^{-1} and ICE from 47%–48% to 67%–68% [145]. Increasing the PT above 1300°C is not always beneficial for bio-HC. At this temperature, the C structure is characterized by an increased graphitic order and a corresponding reduced d-spacing. Moreover, the volume of closed and open pores can decrease, directly impacting the Na^+ insertion/adsorption [57, 144, 146, 147]. Pomegranate-peel HC shows a trend to graphitization and loss of beneficial surface structure at 1200°C–1300°C, with graphite-like smooth sheets and poorer Na

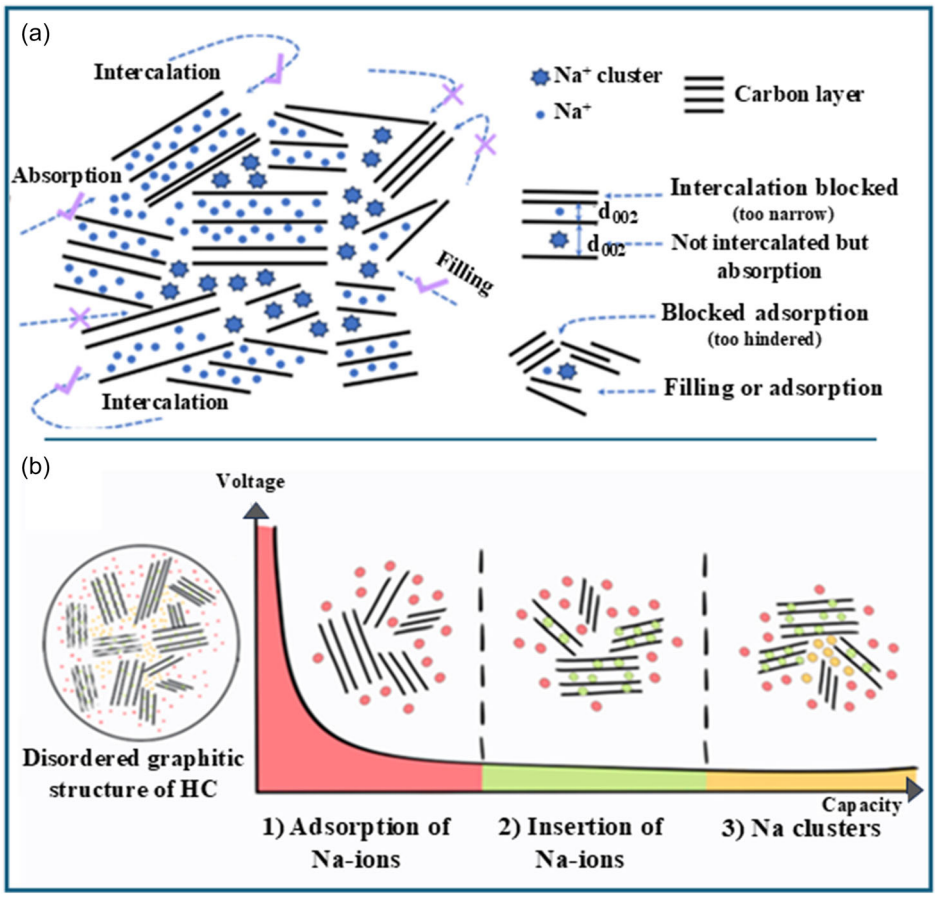

FIGURE 6 | Sodium-ion intercalation mechanisms. In (a) interaction of Na^+ ions within the complex structure of HC anodes. Adapted from [140], permission requested. In (b) the electrochemical correlation of Na^+ ions storage mechanism: adsorption on pores, edges, and defects, insertion into turbostratic domains, and clustering of ions in micropores. Adapted from [141], Creative Commons CC-BY license.

performance [142]. Overall, when *d*-spacing falls below ~0.36 nm, Na^+ intercalation is strongly hindered with concomitant plateau capacity drop [57].

This behavior is illustrated in banana-peel-derived carbons, where increasing carbonization temperature markedly improves reversible capacity and kinetics (e.g., high-temperature HC achieving ~357 mAh g^{-1} versus ~142 mAh g^{-1} at lower temperature), consistent with reduced charge-transfer resistance and removal of electrochemically inactive moieties [148]. Similar optimization windows are observed for wheat-straw-derived HC (≈280 mAh g^{-1} over 200 cycles at 0.1 A g^{-1}), where the best performance reflects a balance between pore development and conductivity rather than maximization of any single structural metric [45].

Among reported biochar-derived anodes, one of the highest sodium-storage capacities was achieved by Sun et al., who developed a lotus stem–derived porous carbon featuring a nanowire framework decorated with graphene quantum dots (GQDs) [149]. Synthesized at 700°C via a self-templating strategy, the material exhibited an exceptionally high surface area (~1574 m^2 g^{-1}) and delivered a reversible capacity of ~460 mAh g^{-1} at 0.2 C after 300 cycles, albeit with a relatively low ICE (~50%). The outstanding performance was attributed to dominant capacitive-controlled storage, fast Na^+ diffusion pathways, and effective accommodation of volume changes during cycling.

Comparable high-capacity behavior was reported by Zhang et al. for a nitrogen-doped HC (N-ZAHC) derived from kapok fibers. This material was engineered via a pre-crosslinking and precarbonization strategy to retain pyridinic-N species during high-temperature pyrolysis [140]. The optimized N-ZAHC anode delivered a reversible capacity of 401.7 mAh g^{-1} at 0.05 A g^{-1} with an ICE of 75.9%, benefiting from enlarged interlayer spacing (~0.387 nm), moderate SSA (~319 m^2 g^{-1}), controlled mesoporosity, and carbonyl-rich surface chemistry. These features collectively stabilized the SEI and enhanced Na^+ storage.

From the reviewed literature, practical guidelines can be derived for the optimization of biochar for NIB anodes. The primary objective is to achieve expanded but not collapsed carbon layers, abundant but controlled closed pores, and moderate defect/heteroatom levels, thereby enabling high capacity, improved ICE, and long-term cycling stability. Generally, the intermediate temperature range (1000°C–1300°C) is the most suitable but requires an empirical tuning of the exact temperature for each specific precursor. For example, corncob and pinenut-derived carbons benefit from pyrolysis around 1300°C–1400°C, whereas pomegranate peel and many nut/wood precursors perform optimally at 1100°C–1200°C [57, 142, 144, 145, 147]. The interlayer spacing and graphitization must be controlled, aiming for d_{002} ~0.36–0.39 nm to balance Na^+ intercalation plateau capacity and structural stability while avoiding overgraphitization ($d_{002} < 0.36$ nm), which sharply reduces plateau capacity. In addition, the closed

pore structure is important for high plateau capacity via the adsorption-filling mechanism. At the same time, open microporosity must be controlled since directly related to SSA, low ICE, and thicker SEI growth.

Pretreatments and activations processes can remove impurities, tune volatile content, and favor the formation of disordered matrices that later develop optimal *d*-spacing and porosity under high temperature pyrolysis [57, 145, 150–153]. Lastly, two-step or staged pyrolysis (low-T precarbonization followed by higher-T treatment) is important to optimize interlayer spacing, lattice ordering, and pore development while retaining structural robustness [57]. A summary of the influence of carbonization temperature on structure/Na-storage behavior is reported in Table 3.

Beyond temperature control, pretreatment strategies such as acid washing and hydrothermal carbonization (HTC) are increasingly employed to improve reproducibility and ICE by moderating surface area and removing ash or metal impurities that destabilize the SEI. Hydrothermal pretreatment prior to high-temperature pyrolysis has been shown to increase carbon yield, tailor microporosity, and deliver ICE values of ~70%–76% with stable cycling over hundreds of cycles [154, 155]. Recent advances further demonstrate that targeted microtexture engineering, particularly closed-pore design, can simultaneously enhance capacity and ICE. Deliberate conversion of open pores into closed micropores reduces electrolyte accessibility, mitigates irreversible reactions, and promotes Na^+ clustering within confined domains, yielding reversible capacities approaching ~385 mAh g^{-1} with ICE up to ~88% [156]. In parallel, scalable activation strategies are evolving beyond conventional KOH-based protocols. Milder chemical activators, such as K_2CO_3, or templating can produce interconnected microporosity while retaining a modest fraction of closed pores, balancing high capacity and electrochemical stability.

For instance, hemp-hurd-derived HC activated with K_2CO_3 and carbonized at ~800°C exhibits a favorable combination of electrochemical properties: an ICE of ~73%, a reversible capacity of ~267 mAh g^{-1} at low current, high-rate performance of ~79 mAh g^{-1} at high current, and strong capacity retention (~96% after 300 cycles at 2 A g^{-1}) [157]. Similarly, morphology-controlled HC from the same precursor, tubular, sheet, or spherical, demonstrate that microstructure, rather than feedstock alone, governs ICE and cycling stability. Tubular architectures with enlarged d_{002} (~0.37 nm) and moderated surface area can achieve reversible capacities of ~265 mAh g^{-1} with ICE ~76%–77% and long-term stability over hundreds of cycles (Figure 7) [154]. A key criticism of field maturation is the increasing frequency of full-cell demonstrations and electrolyte-aware designs. Honeycomb-like, salt-templated biochars with controlled heteroatom content and optimized electrolyte chemistry have achieved high ICE (~86%) and excellent high-rate stability, sustaining thousands of cycles with >95% capacity retention, while full cells reaching energy densities on the order of ~180 Wh kg^{-1} with sodium vanadium phosphate ($Na_3V_2(PO_4)_3$)-based cathodes [158]. Complementary approaches, such as acid washing and temperature optimization (e.g., pomegranate-peel HC carbonized at ~1100°C), reinforce a central design principle: an optimal carbonization window exists, in which d_{002}, oxygen speciation, and surface area collectively maximize reversible capacity without sacrificing ICE [142]. Exceeding this window can reduce slope-region capacity by removing functional sites and decreasing interlayer spacing.

Beyond pure HC, biochar-derived composites are being explored to provide faradaic contributions or improve kinetics. For instance, SnO_2/carbon hybrids and porous biochars have been used as selenium hosts in lithium–selenium (Li–Se) and sodium–selenium (Na–Se) systems, where hierarchical porosity and high surface area enable high Se loading and long-cycle stability [159]. Likewise, lotus-stem-derived porous carbons with embedded graphene quantum dots (GQDs) achieve high capacities in both LIBs and NIBs, although the frequently observed low ICE (~50% for high-surface-area architectures) reinforces the need for practicality-aware benchmarking (see Table 4).

Despite rapid progress, three limitations continue to define the translation gap for biomass-derived HCs in NIBs: (i) ICE and electrolyte consumption remain the dominant barrier, particularly for high-surface-area carbons where SEI formation dominates early cycling [159]. Closed-pore engineering and surface-area control are therefore non-negotiable for practical deployment. (ii) Feedstock variability and ash chemistry translate into batch-to-batch dispersion in microtexture and SEI behavior. Pretreatment, demineralization and standardized pyrolysis protocols are essential to industrial relevance. (iii) Practical cell validation is still uneven. Many reports remain half-cell, low-loading demonstrations; broader adoption requires systematic testing at areal loadings ≥2 mg cm^{-2}, realistic N/P ratios, lean electrolyte, and full-cell configurations [141, 154, 160]

Overall, biochar-derived HC are uniquely aligned with the mechanistic requirements of sodium storage. Their nongraphitizable turbostratic framework, enlarged interlayer spacing, and engineerable porosity enable adsorption–insertion–pore-filling behavior inaccessible to graphite. The most credible pathway forward is co-optimization rather than maximizing a single metric (surface area, d_{0021}, or doping level): closed-pore fraction, oxygen/nitrogen speciation, and active surface area must be

TABLE 3 | Effects of carbonization temperature on biomass structure and Na^+ storage behavior.

Temperature range	Structural changes	Electrochemical impact	Ref.
700°C–900°C	Disordered, high defects/O, high SSA, incomplete carbonization	Higher surface capacity, low ICE, poorer long-term stability	[57, 142, 143, 146]
1000°C–1300°C	Expanded d-spacing (~0.36–0.39 nm), moderate defects, controlled porosity	High reversible capacity, improved ICE, good rate and cycling	[57, 142, 144, 145, 147]
>1300°C	More graphitic, reduced *d*-spacing, loss of useful porosity	Lower Na^+ intercalation/adsorption, capacity decline despite higher ICE	[57, 142, 144–147]

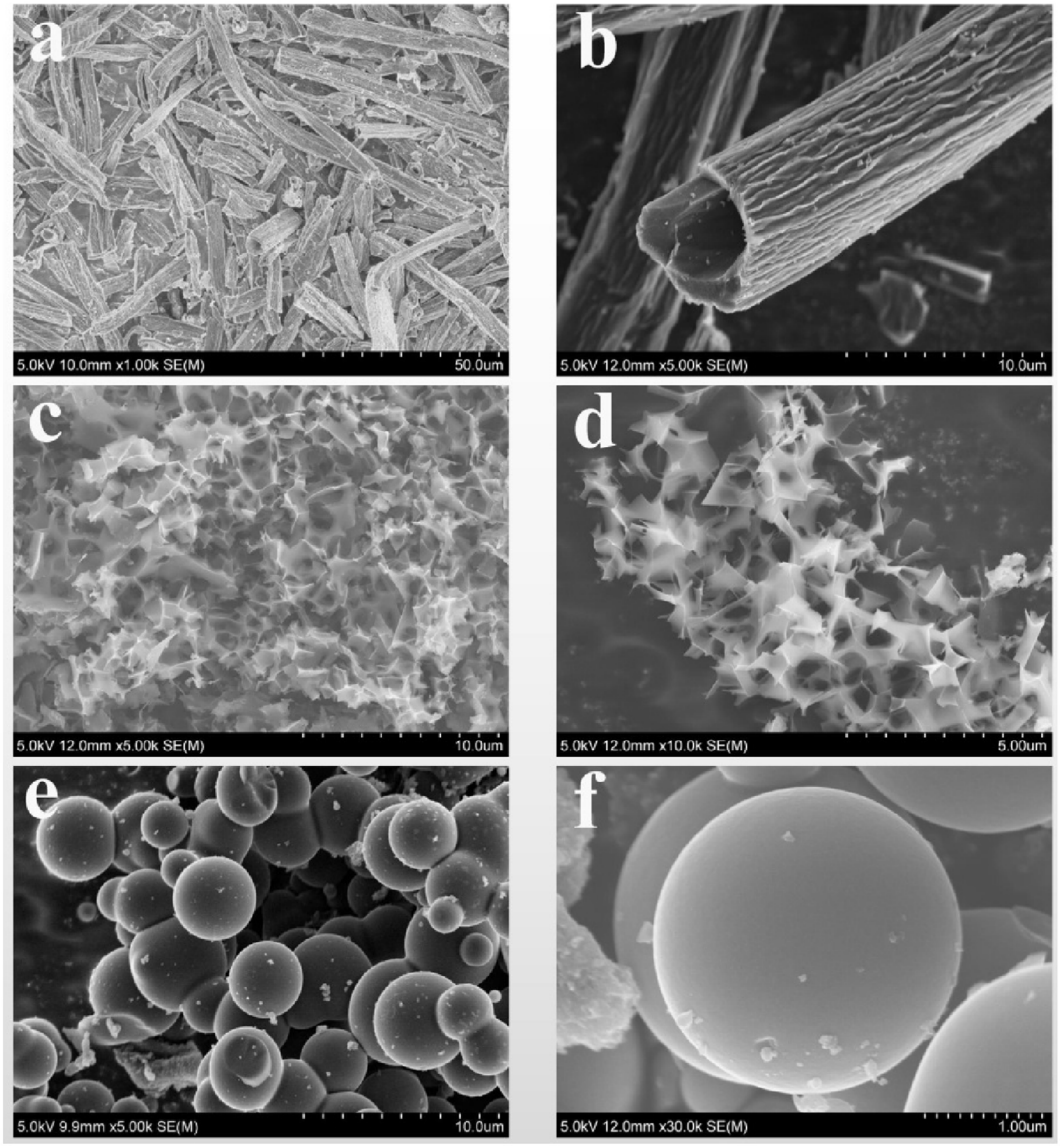

FIGURE 7 | Different morphologies of the same precursor (sisal fiber) but different pretreatment before pyrolysis at 900°C, 1 h in N_2 atmosphere. (a,b) Tubular (TSFC) prepared with HTC treatment in KOH, 160°C, 14h; (c,d) sheet (SSFC) where the HTC in KOH was followed by heating and stirring (80°C) the sample with 2.5 mol L^{-1} KOH solution before pyrolysis; (e,f) spherical (GSFC) prepared with HTC in HCl solution at 180°C for 12 h. Reproduced from [154], Creative Commons CC-BY license.

balanced under realistic electrochemical protocols. In this context, NIBs represent a natural technological landing zone for biochar-based anodes and a proving ground for scalable, circular carbon manufacturing.

3.3 | KIBs

Following the first demonstrations of reversible potassium intercalation in graphite in 2015 [169–171], KIBs have rapidly emerged as a promising alternative to lithium-ion systems for large-scale and cost-sensitive energy-storage applications. Although potassium shares key electrochemical similarities with lithium and sodium, its significantly higher natural abundance in the Earth's crust (~1.5 wt%) makes it more appealing from the perspectives of both sustainability and resource security. Figure 8 illustrates the publication growth in KIB research over the past decade.

Several intrinsic characteristics distinguish KIBs from both LIBs and NIBs. First, potassium does not form stable Al–K intermetallic compounds, enabling the use of aluminum current collectors on the anode side instead of copper, with clear benefits in terms of cost and weight reduction [172]. Second, the standard redox potential of the K/K^+ couple (−2.94 V vs. SHE) lies between Li/Li^+ and Na/Na^+, allowing KIBs to achieve higher operating voltages and, in principle, higher energy densities than sodium-based systems. Third, although K^+ possesses a larger bare ionic radius than Li^+ and Na^+, its weaker solvation leads to a smaller effective Stokes radius in common electrolytes, which translates into faster ionic transport and improved interfacial kinetics [173, 174].

Carbon-based materials dominate anode development for KIBs, including graphite, graphene, and disordered carbons (soft and HC) [173, 174]. Similar to lithium intercalation, potassium can form graphite intercalation compounds (GICs) such as

TABLE 4 | Most relevant biochar-derived carbon used as NIBs electrode material (2023–2025).

Feedstock/ precursor	Processing / Post-treatment	Pyrolysis temperature, °C	Reversible capacity, $mAhg^{-1}$	ICE	Rate capability	Ref.
Pine sawdust	Molten salt pyrolysis ($ZnCl_2$-KCl-NaCl, 1:10 ratio) + HCl washing	500°C, 30min	389 (@2.5C) (Na/Se cathode)	n.d.	300 cycles (@1C), 98% (Na/Se)	[159]
Lotus stem	HTC (water) 180°C, 24h + chemical activation in KOH	700, 2 h	460 (@ 0.2C)	50%	300 cycles (@0.2C), 93%	[149]
Hemp hurd (Cannabis sativa L.)	Prepyrolysis at 500°C + chemical activation with K_2CO_3	800, 1 h	267 (@ 0.03 Ag^{-1})	73%	300 cycles (@2 Ag^{-1}), 96%	[157]
Birch tree waste and SnO_2 composite	HTC (H_3PO_4) 150°C, 16 h	800, 1 h	373 (@ 0.1C)	52%	162 cycles (@0.1 Ag^{-1}), --	[160]
Waste cotton	HTC (KOH) 250°C, 4 h	800, 2 h (char/KOH mixtures)	330 (@ 0.1 Ag^{-1})	79%	400 cycles (@1 Ag^{-1}), 96%	[141]
Sisal fiber	HTC (KOH)160°C, 14 h	900, 1 h	265.2 (@ 0.1 A g^{-1})	76.70%	400 cycles (@ 0.05 Ag^{-1}), 99%	[154]
Aegle marmelos shell	HTC (H_2SO_4) RT, 2 h, 200°C, 48 h	900, 1000	223 (900°C), 212 (1000°C) (@ 0.01 Ag^{-1})	99%	2500 cycles (@1 Ag^{-1}), 68% (900°C), 86% (1000°C)	[161]
Poplar tree biomass tar (N-doped)	N-doping with urea	1000, 1.5 h	257.5 (@ 0.025 Ag^{-1})	59.30%	200 cycles (@1 Ag^{-1}), 70.3%	[162]
Xanthium sibiricum fruit (honeycomb biochar)	NaCl template, prepyrolysis at 600°C	1000, 2 h	161 (@ 4.0 Ag^{-1})	86.50%	3000 cycles (@2.0 Ag^{-1}), 97%	[158]
Pomegranate peel	Acid washing with HCl and HF	1100, 2 h	330 (@ 0.1C)	45%	200 cycles (@0.5C), 68%	[142]
Vine shoots	Precarbonization at 500°C + HCl washing	1200, 2 h	259 (@ 0.03 Ag^{-1})	71%	315 cycles (@0.1 Ag^{-1}), 97%	[45]
Sunflower seed shell	HTC (water) 250°C, 24 h	1200, 2 h	280 (@ C/15)	76%	500 cycles (@1C = 372 $mAhg^{-1}$), 86%	[155]
Spent coffee grounds	HTC (water) 250°C, 24 h	1200, 2 h	240 (@ C/15)	40%	500 cycles (@1C = 372 $mAhg^{-1}$), 85%	[155]
Rose stems	HTC (water) 250°C, 24 h	1200, 2 h	210 (@ C/15)	35%	500 cycles (@1C = 372 $mAhg^{-1}$), 74.5%	[155]
Kapok fiber (N-doped)	$ZnCl_2$-assisted pre-cross-linking, precarbonization with $C_7H_5NO_4$ at 220°C	1200, 2 h	401.7 (@ 0.05 A/g)	76%	500 cycles (@0.4Ag^{-1}), 98%	[140]
Walnut shell + polystyrene	Two prepyrolysis at 1000°C and 700°C adding polystyrene	1200, 2 h	385 (@ 0.05 Ag^{-1})	88%	300 cycles (@1Ag^{-1}), 99.9%	[156]

(Continues)

TABLE 4 | (Continued)

Feedstock/ precursor	Processing / Post-treatment	Pyrolysis temperature, °C	Reversible capacity, $mAhg^{-1}$	ICE	Rate capability	Ref.
Sorghum husk	N-doped with HTC (HNO_3) post treatment, 180°C, 6 h	1200, --	322 (@ 0.05 Ag^{-1}, −20°C)	91%	600 cycles (@1 Ag^{-1}), --	[163]
Basswood	Bacterial/enzymatic tailoring	300, 2 h + 1300 for other 5h	366.4 (@ 0.02 Ag^{-1})	88.20%	200 cycles (@0.1 Ag^{-1}), 98.8%	[164]
wasted Sulfuric acid paper	H_2SO_4 washing + preoxidation at 300°C, 4 h in air	1400, 2 h	350.1 (@ 0.03 Ag^{-1})	77.30%	100 cycles (@ 0.3 Ag^{-1}), 80.7%	[165]
Metaplexis japonica seed hair fibers	Prepyrolysis at 500°C in N_2 + HCl washing	1400, 2 h	331.7 (@ 0.03 Ag^{-1}), 229 (@ 3 Ag^{-1})	94.8% (@0.03 Ag^{-1})	2000 cycles (@2 Ag^{-1}), 84.1%	[166]
Cellulose	None	1500, 1 h	308 (@ 0.0372 Ag^{-1})	87%	50 cycles (@0.0372 Ag^{-1}), 95%	[167]
Lignin	None	1500, 1 h	273 (@ 0.0372 Ag^{-1})	80%	50 cycles (@0.0372 Ag^{-1}), 95%	[167]
Chitosan	None	1500, 1 h	256 (@ 0.0372 $Ag^{-1)}$	86%	50 cycles (@0.0372 Ag^{-1}), 96%	[167]
Potato starch	Stabilization in air, 200°C, 3 days	1500, 1 h	291 (@ 0.0372Ag^{-1})	89%	50 cycles (@0.0372 Ag^{-1}), 92%	[167]
Rice starch	Stabilization in air, 200°C, 3 days	1500, 1 h	39 (@ 0.0372 Ag^{-1})	85.80%	50 cycles (@0.0372 Ag^{-1}), 92%	[167]
Pine nut shells	Oxygen functionalization via O2 pyrolysis at 400°C + carbonization via N_2 pyrolysis at 400°C	1500, 2 h (char/ KOH mixture)	378.1 (@ 0.1C)	88%	200 cycles (@1.5 Ag^{-1}, (5C)), 85.2%	[139]
Black locust wood	6M HCl pretreatment	500, 2 h + 1500 for other 2 h	382 (@ 0.1C)	67%	100 cycles (@ 0.3C), 90%	[168]

Abbreviations: K_2CO_3, potassium carbonate; KOH, potassium hydroxide; NaCl, sodium chloride; $ZnCl_2$, zinc chloride.

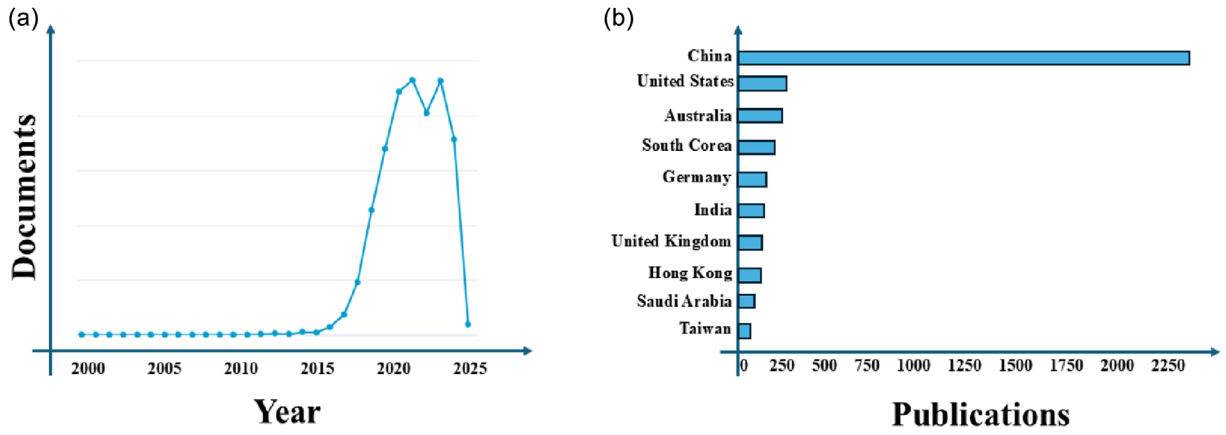

FIGURE 8 | Publication trends in potassium-ion battery research from 2015 to 2024. Data retrieved from the Scopus database (Elsevier) using the query "potassium-ion battery" and "carbon anode." Figure adapted and reprocessed by the authors. In (a) the annual number of published documents. In (b) the distribution of publication output by country, highlighting the relative contribution of major producing nations.

KC_{36}, KC_{24}, and KC_8, yielding a theoretical capacity of 279 mAh g^{-1} [172]. However, graphite suffers from severe structural instability during K^+ intercalation. The graphite interlayer spacing expands from 0.335 to ~0.530 nm, corresponding to a ~63% volumetric expansion. This drastic lattice dilation promotes exfoliation, structural collapse, and rapid capacity fading upon repeated cycling. Consequently, strategies including interlayer spacing modification, heteroatom doping, surface engineering, and morphology optimization have been extensively explored to mitigate these intrinsic limitations [175, 176]. Achieving high performance while maintaining mechanical integrity remains a central challenge in KIB anode design.

In this context, biochar-derived and biomass-based HC represent a structurally superior platform for potassium storage [177]. Their turbostratic, nongraphitisable frameworks possess intrinsically enlarged interlayer spacing and disordered pore networks capable of accommodating large K^+ ions. Closed nanopores further function as mechanical buffers, alleviating stress during repeated insertion–extraction cycles.

Compared to LIBs and NIBs, biochar-derived HCs face more pronounced limitations in KIBs. The larger ionic radius and higher mass of K^+ slow diffusion and promote steric hindrance within disordered carbon frameworks, leading to channel blockage and faster capacity decay [178–180]. Additionally, the typically higher ash content and heteroatom-rich surface of biochar intensify side reactions. Due to the higher reactivity of K^+, this results in thicker and less stable SEI layers, increased polarization, and progressive interfacial degradation [150, 178–180]. While microporosity enhances capacity in LIBs and NIBs, in KIBs it promotes irreversible K^+ trapping and electrolyte confinement, lowering ICE and accelerating capacity fading [178, 179].

Electrochemically, potassium storage in HC mirrors the behavior observed in sodium-ion systems. Galvanostatic profiles typically display two distinct regions: a higher potential sloping region associated with K^+ adsorption on surface defects, edges, and heteroatom sites, followed by a lower potential plateau attributed to interlayer insertion and pore-filling processes. This multimechanism storage enables higher reversible capacity and improved cycling stability compared to crystalline graphite.

To optimize these properties, a variety of synthetic strategies have been explored, largely paralleling those developed for SIBs. These include single- and multistep pyrolysis, hydrothermal carbonization (HTC), salt-templating, chemical activation, and heteroatom doping (notably N, O, P, and S). Such approaches enable precise control over interlayer spacing, defect density, electronic conductivity, and pore architecture, all critical parameters for efficient K^+ storage.

Among reported studies, outstanding cycling stability was achieved by Wang et al. [181], who synthesized an N-doped HC derived from lignin using Zn-assisted multistep pyrolysis under Ar/H_2 at 1100°C, followed by ammonia activation at 800°C. The resulting material (denoted on-CZL) demonstrated exceptional durability, sustaining 10,000 charge–discharge cycles at a high current density of 5 A g^{-1}. This performance was attributed to a synergistic combination of factors: (i) a large interlayer spacing of ~0.44 nm dictated by the lignin precursor; (ii) Zn vapor-induced expansion and restructuring of graphitic domains; (iii) Zn-catalyzed cross-linking effects that promote curvature and turbostratic disorder; and (iv) nitrogen doping, which further modulates interlayer spacing and electronic structure.

An alternative morphological strategy was proposed by Wang et al. [182], who prepared MnO_4 as a sacrificial template to construct a nanotube-like carbon architecture. This material delivered a reversible capacity as high as 407 mAh g^{-1} at 0.1 A g^{-1}, representing one of the highest values reported for carbonaceous KIB anodes to date. The enhanced performance was attributed to the combination of high accessible surface area, shortened diffusion pathways, and structural resilience against volume expansion.

Overall, these studies demonstrate that biochar-derived and HC offer decisive advantages over graphite for potassium-ion storage, provided that their microstructure, chemistry, and morphology are rationally engineered. A comprehensive overview of biochar- and biomass-derived HC anodes for KIBs, including synthesis routes, structural parameters, and electrochemical performance metrics, is provided in Table 5.

3.4 | Correlations Across Alkali-Ion Systems

A systematic correlation emerges across alkali-ion battery systems as the ionic radius increases (Li^+, 0.76 Å < Na^+,

TABLE 5 | Summary of the most relevant biochar-derived carbon used as KIBs electrode material (2023–2025). HTC, hydrothermal carbonization.

Biowaste precursor	Processing/ Modification	Pyrolysis temperature, °C	Reversible capacity, $mAhg^{-1}$	ICE	Performance	Ref.
Cellulose nanofiber and coal tar pitch	Solution mixing of cellulose and coal tar pitch	1200	366 (@ $0.03Ag^{-1}$)	n.d.	1000 cycles (@$1\,Ag^{-1}$), 74.2%	[183]
Pinus massoniana bark	Ore-oxidation at 250°C, 4 h + HTC (water) 180°C, 12 h + ball milling post pyrolysis	600, 3 h	256.1 (@ $0.1Ag^{-1}$)	46%	3000 cycles (@$1\,Ag^{-1}$), 80%	[184]
Calophyllum inophyllum L. (N-doped)	Ball milling + wet impregnation urea + HCl washing after pyrolysis	1200, 3 h	208.9 (@ 0.05 Ag^{-1})	59%	1000 cycles (@0.5 Ag^{-1}), --	[185]
Lignite + Starch	Ball milling + preoxidation at 260°C, 2 h in air	1300, 1 h	284.9 (@ 0.1C)	74%	500 cycles (@1C), 92.2%	[186]
Coffee waste + Graphene	Mixture freeze-dried for 3 days, ball milling after pyrolysis	950, 1 h	175 (@ 0.1C)	n.d.	300 cycles (@1C), >80%	[187]
Sorghum biomass (N-S-doped)	Delignification with NaOH, copyrolysis with thiourea for doping	600, 1 h	268 (@ 0.1 A g^{-1})	60%	2400 cycles (@ $1\,Ag^{-1}$), high	[188]
Kigelia africana fruit	HCl washing after pyrolysis	1100, 2 h	230 (@ 0.02 Ag^{-1})	42%	200 cycles (@$0.2\,Ag^{-1}$), 83.7%	[189]
Black liquor + Deinking sludge (paper mill waste)	HCl pretreatment + ball milling with pore enlarging agent	800, 3 h	303.5 (@ 0.05 Ag^{-1})	n.d.	500 cycles (@$2\,Ag^{-1}$)	[190]
Poplar fallen leaves	HTC (water) 200°C, 10 h + HCl washing + KOH washing + ball milling after pyrolysis	1300, 3 h	283.3 (@ 0.02 Ag^{-1})	84.2%	550 cycles (@0.1 Ag^{-1}), 76%	[191]
Organic carbon	MnO_2 template + citric acid final washing	900, 2 h	407 (@$0.1\,Ag^{-1}$)	48%	200 cycles (@$0.1\,Ag^{-1}$), 94.8%	[182]
Boron-doped glucose	HTC (boric acid) 200°C, 12 h	1200, 2 h	361 (@$0.03\,Ag^{-1}$)	n.d.	800 cycles (@$1\,Ag^{-1}$), 70.5%	[192]
Coconut shell	HTC (water) 200°C, 12 h + ball milling + HCl washing	1300, 3 h	280 (@$0.05\,Ag^{-1}$)	87%	100 cycles (@ $0.05\,Ag^{-1}$), 92.8%	[193]
Wedelia chinensis	Ethanol soaking, 12 h	800, 2 h	350 (@$0.1\,Ag^{-1}$)	50%	500 cycles (@$0.1\,Ag^{-1}$), low	[194]
Tender coconut peels + reduced Graphene Oxide	Prepyrolisis at 500°C, 5 h + HCl washing post pyrolysis	1100, 5 h	321.7 (@$0.03\,Ag^{-1}$)	84%	600 cycles (@$0.2Ahg^{-1}$), 15.6%	[195]
Pinecone (N-doped)	Fe_2O_3 composite, nitric acid activation 70°C, 5 h	HTC 150°C, 30 h	178.7 (@0.05 A/g)	76%	500 cycles (@$0.5Ag^{-1}$), 83.4%	[196]

(Continues)

TABLE 5 | (Continued)

Biowaste precursor	Processing/ Modification	Pyrolysis temperature, °C	Reversible capacity, $mAhg^{-1}$	ICE	Performance	Ref.
Lignin (N-doped)	Zn powder assisted multistep pyrolysis: Ar/H_2; NH_3	1100, 2 h; 800, 30min	303 (@1 Ag^{-1})	26%	10 000 cycles (@5 Ag^{-1})	[181]
Sisal hemp	HTC(HCl) 160°C, 12 h + hydrazine hydrate 120°C, 12 h	1300, 2 h	310 (@0.1C)	n.d.	1000 cycles (@1C), 64.2%	[197]
D-Xylose (inedible lignocellulosicbiomass)	$FeCl_3$ +KOH solution, multistep pyrolysis + HCl washing	120, 2 h; 600, 2 h; 1000, 4 h	301 (@0.1 Ag^{-1})	n.d.	1700 cycles (@0.5Ag^{-1}), 79.2%	[198]
Platanus occidentalis L. fruit	Pretratment at 400°C, 2 h in Ar + HCl washing after pyrolysis	800, 2 h	234.2 (@0.1 Ag^{-1})	63.7%	300 cycles (@ 0.3 Ag^{-1})	[199]
Camphor leaf residue (P-doped)	Sodium phytate mixture, HTC (water) 180°C, 12 h, pressed before pyrolysis, HCl washing after pyrolysis	1400, 2 h	275.4 (@0.1 Ag^{-1})	33%	500 cycles (@0.1 Ag^{-1})	[200]
Corn stalks, corn cobs and corn leaves	HCl washing after pyrolysis	800, 2 h	110 (@ 0.05 Ag^{-1})	n.d.	800 cycles (@0.2 Ag^{-1})	[201]
Corn stalks, corn cobs and corn leaves	KOH washing after pyrolysis	800, 2 h	151 (@ 0.05Ag^{-1})	n.d.	800 cycles (@0.2 Ag^{-1})	[201]
Corn stalks, corn cobs and corn leaves (N-P-S-doped)	KOH washing + urea/ thiourea/phosphoric acid activation	800, 2 h	225 (@ 0.05Ag^{-1})	n.d.	1000 cycles (@0.2 Ag^{-1})	[201]
sugarcane bagasse	HCl washing	1200, 8 h	235 (@ 0.1 Ag^{-1})	n.d.	2000 cycles (@0.5 Ag^{-1}), --	[202]
Rhus typhina wood	Ethanol soaking, 12 h + HTC (water) 180°C, 10 h; KOH second pyrolysis	500, 1h	108.4 (@ 0.2C)	n.d.	1000 cycles (@0.2C), --	[203]

1.02 Å < K^+, 1.38 Å): the dominant storage mechanism progressively shifts from intercalation-controlled behavior toward defect-mediated adsorption and pore filling [204]. This transition fundamentally alters the structural requirements of carbon anodes and explains why graphite remains optimal for LIBs but fails for NIBs and performs only marginally in KIBs [205].

In LIBs, lithium readily intercalates into the well-ordered graphene layers of graphite via a staged mechanism (LiC_6), delivering a theoretical capacity of 372 mAh g^{-1} with high ICE (>90% in commercial systems) [206]. Consequently, high structural ordering, low surface area, and minimal defect density are essential to suppress irreversible lithium trapping and excessive SEI formation. Hard carbons and biochars with large surface areas often exhibit high apparent capacities (>400 mAh g^{-1}), but these are frequently dominated by surface adsorption and pseudocapacitive contributions, which compromise ICE and volumetric energy density [125]. Thus, for LIB applications, biochar must approach a graphite-mimetic architecture, moderate turbostratic stacking, reduced heteroatom content, and controlled porosity to achieve competitive practical performance.

In contrast, sodium ions do not form stable graphite intercalation compounds under standard conditions due to thermodynamic and kinetic limitations associated with their larger ionic radius and weaker binding to graphene layers [126]. Instead, sodium storage in HC proceeds through a hybrid mechanism, as already described in Section 3.2; in this case, controlled disorder becomes advantageous rather than detrimental. Moderate defect density, expanded interlayer spacing (>0.37 nm), and hierarchical porosity enhance sodium uptake while maintaining cycling stability [207]. Heteroatom doping (e.g., N or O) can further improve Na^+ adsorption energetics and electronic conductivity, often increasing reversible capacity without the severe ICE penalties observed in LIB systems [208]. Consequently, biochar-derived HC materials are particularly well suited to NIB systems, where their intrinsic turbostratic structure aligns with the required storage mechanism. The trend becomes even more pronounced in potassium-ion batteries.

The larger ionic radius of K^+ and its lower Lewis acidity favor surface-controlled storage and capacitive contributions over classical intercalation [171]. While graphite can reversibly host potassium via KC_8 formation, the associated volume expansion and sluggish diffusion limit long-term stability [169]. In disordered carbons, potassium storage is strongly influenced by defect density, pore accessibility, and surface chemistry [209]. Larger mesopores facilitate ion transport, while oxygen- and nitrogen-containing functional groups enhance adsorption kinetics and capacitive contributions [210]. As a result, highly porous biochars that would be suboptimal for LIBs may exhibit competitive performance in KIBs, particularly at high rates.

Across the three systems, therefore, a clear materials-design gradient can be identified:

- LIBs favor structural order, low surface area, and graphite-like staging behavior.
- NIBs benefit from turbostratic HC with controlled microporosity and moderate defect density.
- KIBs increasingly favor defect-rich, hierarchical porous carbons enabling surface-dominated storage.

Importantly, heteroatom functionalities exhibit opposite effects depending on the ion: in LIBs, they often reduce ICE due to irreversible lithium consumption during SEI formation, whereas in NIBs and KIBs, they can enhance adsorption energy and capacitive charge storage [208, 210]. This inversion underscores that biochar optimization cannot be universally graphite-mimetic but must be tailored to the specific ionic species and its associated thermodynamic and transport constraints.

Taken together, these correlations demonstrate that the intrinsic structural plasticity of biochar, tunable interlayer spacing, defect density, and surface chemistry via pyrolysis engineering provide a versatile platform adaptable across alkali systems. However, the optimal carbon architecture shifts systematically with ionic radius, necessitating ion-specific design strategies rather than a single universal carbon blueprint.

3.5 | Role of Heteroatom Doping in Modulating Alkali-Ion Storage Mechanisms

Heteroatom doping represents one of the most effective strategies for tailoring the electrochemical behavior of biochar-derived HCs, yet its impact is intrinsically ion-dependent. The incorporation of heteroatoms such as N, P, S, or B modifies the electronic structure, local bonding configuration, and defect topology of the carbon matrix, thereby altering both bulk transport properties and interfacial reactivity. Importantly, doping does not simply increase capacity; it reshapes the dominant storage mechanism by tuning adsorption energetics, interlayer spacing, and surface chemistry. The standard doping procedure relies on heteroatom incorporation during high-temperature pyrolysis. However, an appropriate synthesis strategy can be implemented to select specific functional groups [211].

From an electronic standpoint, substitutional or edge-site heteroatoms perturb the π-conjugated carbon network by donating or withdrawing electron density, increasing carrier concentration and reducing charge-transfer resistance [57, 212–214]. These effects are particularly relevant for rate performance and high-power operation. Structurally, heteroatom incorporation can expand interlayer spacing, distort graphitic domains, and promote the formation of micro- and mesopores, facilitating the accommodation of larger alkali ions and increasing the density of redox-active sites [213]. Simultaneously, polar functional groups enhance electrolyte wettability and promote surface-dominated, pseudocapacitive contributions [212, 215].

However, the role of heteroatoms is not universally beneficial and must be interpreted within the ion-specific context. In LIBs, excessive defect density and surface functionality can amplify irreversible lithium consumption during SEI formation, reducing ICE. While moderate N-doping may enhance conductivity and kinetics, overly reactive surfaces are detrimental in systems where intercalation-dominated storage is already highly efficient. Thus, for lithium chemistry, doping must be restrained and carefully controlled.

In contrast, NIBs benefit more directly from heteroatom incorporation. Because sodium storage relies on a hybrid mechanism combining interlayer insertion and adsorption within nanopores, controlled expansion of d-spacing and enhanced surface polarity can significantly increase reversible capacity. This behavior is reflected in several representative studies. For example, N-doping

of pinecone-derived HC increased reversible capacity from 197 to 273 mAh g^{-1} with ~80% capacity retention after 250 cycles, attributed to improved electronic conductivity and additional adsorption sites [146]. Phosphorus incorporation into spherical HC expanded interlayer spacing and enhanced the low-voltage plateau contribution, delivering 343 mAh g^{-1} with 92% ICE [216]. Likewise, N/P codoping has demonstrated the possibility of simultaneously enlarging *d*-spacing and stabilizing defect structures, achieving 336 mAh g^{-1} with 99.8% capacity retention over 2000 cycles [217]. These examples illustrate that heteroatom engineering in NIBs functions not merely as defect introduction, but as controlled modulation of turbostratic order and sodium adsorption energetics.

For KIBs, the impact of heteroatom doping becomes even more nuanced. The large ionic radius and lower charge density of K^+ favor surface-controlled storage and adsorption processes, suggesting that polar heteroatom sites could enhance ion affinity and capacitive contributions. At the same time, the higher chemical reactivity of potassium exacerbates interfacial instability, meaning that excessive functionalization may intensify continuous SEI growth and accelerate degradation. Systematic studies specifically addressing doped biochar in KIBs remain limited [214], and a mechanistic understanding of how heteroatom chemistry influences SEI composition and stability in potassium systems is still emerging.

Codoping strategies (e.g., N/S or N/P) introduce additional complexity by generating synergistic electronic and structural effects. While such approaches can create hierarchical defect networks and improved ion diffusion pathways, they may also compromise mechanical integrity or electronic continuity if the defect density becomes excessive. Consequently, the optimization variable is not the absolute heteroatom content but rather its bonding configuration, spatial distribution, and interaction with the carbon backbone.

Overall, heteroatom doping should not be viewed as a universal performance enhancer, but as a precision tool for modulating storage mechanisms in an ion-specific manner. The central challenge moving forward is to identify optimal doping levels and configurations that balance electronic conductivity, defect-mediated capacity, ICE, and long-term interfacial stability. Achieving this balance will require advanced characterization techniques capable of resolving dopant bonding states and local environments, coupled with predictive models that relate dopant chemistry to electrochemical response across different alkali-ion systems.

4 | Current Limitations and Future Perspectives

The correlations outlined in Section 3.4 make one point clear: biochar cannot be optimized using a single structural paradigm across LIBs, NIBs, and KIBs. As the ionic radius increases from Li^+ to K^+, the dominant storage mechanism progressively shifts away from classical intercalation toward adsorption and pore-mediated processes. The practical implication is that the performance ceiling of biochar-derived HC is not intrinsic, but ion-dependent [218].

In LIBs, the limitation is largely thermodynamic and interfacial. Lithium intercalation favors highly ordered graphitic domains with minimal surface reactivity. Biochars, by contrast, inherently possess turbostratic disorder, residual heteroatoms, and significant surface area. While these features can inflate specific capacity through adsorption contributions, they simultaneously intensify SEI formation and depress ICE [219]. For lithium systems, where ICE, volumetric density, and long-term stability are already optimized in commercial graphite [220], the tolerance for surface-driven storage is low. Thus, biochar must approach graphite-like behavior to be competitive, which paradoxically reduces the very structural complexity that makes it attractive.

For NIBs, the situation is more favorable but not unconstrained. Sodium does not intercalate efficiently into graphite under standard conditions, making turbostratic HCs intrinsically suitable. However, performance is highly sensitive to interlayer spacing and pore topology. If spacing is insufficient, plateau capacity collapses; if microporosity is excessive, irreversible Na^+ trapping increases and ICE deteriorates [221]. The challenge is therefore not simply introducing disorder but controlling it with precision.

In KIBs, the constraints become more severe and more interfacial in nature. The large ionic radius and high reactivity of K^+ amplify steric limitations and electrolyte decomposition. Even when structural diffusion pathways are adequate, interfacial instability dominates cycling behavior. Thick, continuously evolving SEI layers and increased polarization accelerate degradation [222]. Highly porous carbons may show attractive rate capability, yet excessive defect density intensifies irreversible trapping and side reactions. Here, interfacial engineering, not merely pore optimization, becomes decisive.

Across all systems, several structural trade-offs persist. Increasing surface area enhances ion accessibility but proportionally increases irreversible alkali consumption. Raising PT improves conductivity and structural stability yet narrows interlayer spacing and suppresses defect-mediated storage [223]. No single metric, whether Raman I_D/I_G, d_{002} spacing, or BET surface area, adequately predicts performance. What is required is coordinated control of spacing, pore hierarchy, defect chemistry, and surface passivation.

A central manifestation of these trade-offs is the limited ICE and long-term cycling stability often observed in biochar-derived carbons. Low ICE primarily arises from extensive SEI formation on high-surface-area, defect-rich structures, irreversible ion trapping within ultramicropores, and side reactions associated with residual functional groups or mineral impurities. Strategies to mitigate these effects include controlled high-temperature pyrolysis to reduce surface reactivity, pore-size optimization to limit ion confinement, surface passivation or artificial SEI layers, and precursor demineralization [67]. Long-term stability challenges, particularly pronounced in KIBs, are instead governed by continuous SEI growth, interfacial instability, and structural degradation under repeated insertion/extraction. Mitigation, therefore, requires balanced defect engineering, hierarchical porosity design, and electrolyte/interphase optimization rather than simply increasing disorder [224].

Beyond materials design, translational barriers remain significant. Benchmarking inconsistency, differences in electrode loading, electrolyte excess, formation protocols, and half-cell configurations continue to obscure meaningful comparison across studies. Without standardized evaluation under practical

conditions (high areal loading, lean electrolyte, full-cell validation), laboratory-scale gains risk being overstated.

Feedstock variability further complicates reproducibility. Differences in lignin content, mineral residues, and inherent heteroatom distribution alter carbonization pathways even under identical thermal profiles, producing divergent microtextures and electrochemical responses [225]. Rational precursor classification and predictive process–structure–performance frameworks are therefore not optional but necessary for scale-up.

Closely related to feedstock variability is the challenge of batch-to-batch reproducibility. Even when precursor type is nominally constant, fluctuations in biomass provenance, seasonal composition, moisture content, and inorganic impurities can subtly modify carbonization kinetics. Additional variability may arise from reactor-scale effects such as thermal gradients, heating-rate fluctuations, residence-time dispersion, or inconsistencies in post-treatment and washing steps [226]. These factors translate into measurable differences in interlayer spacing, defect density, porosity distribution, and residual ash content, ultimately affecting ICE, rate capability, and cycling stability. Achieving industrial relevance, therefore, requires tighter control of precursor conditioning, programmable and monitored pyrolysis protocols, standardized postprocessing, and the development of predictive models capable of reducing empirical variability. Activation strategy further determines both electrochemical performance and scalability. Chemical activation (e.g., KOH, $ZnCl_2$, H_3PO_4) typically generates very high surface area and microporosity, enhancing adsorption-driven capacity, particularly in NIBs and KIBs [227]. However, excessive surface area lowers ICE due to intensified SEI formation and introduces environmental concerns associated with chemical consumption and wastewater treatment. In contrast, physical activation (e.g., CO_2 or steam) enables more moderate porosity development, improved structural stability, and better compatibility with continuous, low-impact thermal processing. From a translational perspective, controlled activation combined with precursor engineering appears more promising than aggressive chemical etching, particularly when integration into waste-valorization or biorefinery infrastructure is considered.

Finally, sustainability must be critically assessed. Some high-capacity carbons rely on aggressive chemical activation or templating routes that are energy-intensive and environmentally burdensome. If the processing footprint outweighs the renewable origin of the precursor, the circular-economy argument weakens. Scalable thermal routes, mild activation strategies, and integration with biorefinery infrastructure represent more credible paths forward.

Biochar should not be framed as a universal graphite replacement. Its value lies in structural adaptability. For LIBs, this adaptability must be restrained; for NIBs, it must be tuned; for KIBs, it must be coupled with interfacial stabilization. Progress will depend less on maximizing surface area and more on understanding how ion size, thermodynamics, and interfacial chemistry redefine the optimal carbon architecture in each system.

5 | Conclusions

Biochar-derived carbons occupy a distinctive position within the carbon materials landscape for EES, combining renewable origin with a level of structural tunability that is difficult to achieve using fossil-derived carbons. While their intrinsic disorder, high surface area, and feedstock-dependent heterogeneity impose clear limitations in LIBs, particularly in terms of ICE and volumetric energy density, these same features become enabling in systems based on larger alkali ions. When rationally engineered, biochar-derived HCs provide the enlarged interlayer spacing, defect chemistry, and pore architecture required for efficient sodium and potassium storage, positioning them as a natural alternative to graphite in next-generation intercalation batteries. The transition from laboratory demonstrations to industrial relevance will depend on the convergence of standardized benchmarking, scalable and low-impact manufacturing, and data-driven optimization of structure–property relationships. Achieving this convergence would allow biochar to evolve from a promising material into a cornerstone of circular, resilient energy-storage technologies.

Author Contributions

Valerio C. A. Ficca: writing – original draft (equal). **Afef Dhaffouli**: writing – original draft (supporting). **Rocco Cancelliere**: conceptualization (lead), visualization (lead), writing – original draft (equal), writing – review and editing (lead).

Acknowledgments

The present work was carried out with the financial support of the Ministry of Environment and Energy Security for funding Project 1.2 (Integrated project on electrochemical and thermal storage technologies), CUP: I53C24003300001 in the framework of "Ricerca di Sistema Elettrico"—PTR25–27.

Open access publishing facilitated by ENEA Agenzia Nazionale per Le Nuove Tecnologie l'Energia e lo Sviluppo Economico Sostenibile, as part of the Wiley - CRUI-CARE agreement.

Funding

This study was supported by Ministry of Environment and Energy Security (Grant CUP: I53C24003300001).

Conflicts of Interest

The authors declare no conflicts of interest.

References

1. M. A. Kipp, "Carbon Cycling: How much Life Has ever Existed on Earth?," *Current Biology* 33 (2023): R1153–R1155, https://doi.org/10.1016/j.cub.2023.09.041.

2. E. Vangioni and M. Cassé, "Cosmic Origin of the Chemical Elements Rarety in Nuclear Astrophysics," *Frontiers in Life Science* 10 (2017): 84–97, https://doi.org/10.1080/21553769.2017.1411838.

3. E. M. Holmbeck, T. M. Sprouse, and M. R. Mumpower, "Nucleosynthesis and Observation of the Heaviest Elements," *The European Physical Journal A* 59 (2023): 28, https://doi.org/10.1140/epja/s10050-023-00927-7.

4. F. Wang, J. D. Harindintwali, Z. Yuan, et al., "Technologies and Perspectives for Achieving Carbon Neutrality," *The Innovation* 2 (2021): 100180, https://doi.org/10.1016/j.xinn.2021.100180.

5. F. Bauer, T. D. Nielsen, L. J. Nilsson, et al., "Plastics and Climate Change—Breaking Carbon Lock-ins through Three Mitigation Pathways," *One Earth* 5 (2022): 361–376, https://doi.org/10.1016/j.oneear.2022.03.007.

6. R. A. Muñoz Meneses, G. Cabrera-Papamija, F. Machuca-Martínez, L. A. Rodríguez, J. E. Diosa, and E. Mosquera-Vargas, "Plastic Recycling and Their use as Raw Material for the Synthesis of Carbonaceous Materials," *Heliyon* 8 (2022): e09028, https://doi.org/10.1016/j.heliyon.2022.e09028.

7. M. T. Rahaman, A. D. Pranta, M. R. Repon, M. S. Ahmed, and T. Islam, "Green Production and Consumption of Textiles and Apparel: Importance, Fabrication, Challenges and Future Prospects," *Journal of Open Innovation: Technology, Market, and Complexity* 10 (2024): 100280, https://doi.org/10.1016/j.joitmc.2024.100280.

8. D. D. Furszyfer Del Rio, B. K. Sovacool, S. Griffiths, et al., "Decarbonizing the Pulp and Paper Industry: A Critical and Systematic Review of Sociotechnical Developments and Policy Options," *Renewable and Sustainable Energy Reviews* 167 (2022): 112706, https://doi.org/10.1016/j.rser.2022.112706.

9. L. Moreau, E. Thiffault, G. Landry, and J.-F. Carle, "How Does Shifting Wood Products between Uses Affect Their Carbon Dynamics and Climatic Impacts? Leveraging MoSiR, a New Carbon Accounting Tool," *Ecological Modelling* 508 (2025): 111236, https://doi.org/10.1016/j.ecolmodel.2025.111236.

10. X. Xu and B. Lieuea, "Contribution of Modern Renewables to Final Energy Consumption, Energy Intensity, and Environmental Quality: The Role of World Energy Balances, Economic Performance, and Shadow Economies," *Energy* 332 (2025): 137191, https://doi.org/10.1016/j.energy.2025.137191.

11. A. A. Yaroshevsky, "Abundances of Chemical Elements in the Earth's Crust," *Geochemistry International* 44 (2006): 48–55, https://doi.org/10.1134/S001670290601006X.

12. S. Daga, K. Yadav, P. Singh, and V. Mishra," Beyond the Take-Make-Dispose Model—Unlocking the Power of Circular Economy for an Environmentally Resilient Future," *Circular Economy and Environmental Resilience*, ed. P. Singh, S. Daga, K. Yadav, and V. Mishra (Springer Nature Switzerland, 2025). 1–11, https://doi.org/10.1007/978-3-031-93091-1_1.

13. S. A. Neves and A. C. Marques, "Drivers and Barriers in the Transition From a Linear Economy to a Circular Economy," *Journal of Cleaner Production* 341 (2022): 130865, https://doi.org/10.1016/j.jclepro.2022.130865.

14. M. P. Eelager, N. P. Dalbanjan, S. Madihalli, et al., "Pathways to a Sustainable Future: Exploring the Synergy between Sustainability and Circular Economy," *Sustainable Futures* 10 (2025): 101208, https://doi.org/10.1016/j.sftr.2025.101208.

15. R. Kumar, M. Maestri, and V. Ranade, "Sustainable Energy and Decarbonization: Challenges and Opportunities," *Acs Engineering Au* 4 (2024): 290–292, https://doi.org/10.1021/acsengineeringau.4c00013.

16. O. Apata, "Decarbonization Pathways through Multi-Energy System Planning," *Energy Reports* 13 (2025): 4477–4490, https://doi.org/10.1016/j.egyr.2025.04.029.

17. C. Geng, S. Li, J. Li, et al., "Emerging Intercalation-Type Anodes for High-Performance Rechargeable Aqueous Batteries," *Nano Energy* 145 (2025): 111407, https://doi.org/10.1016/j.nanoen.2025.111407.

18. C. Heubner, T. Lein, M. Schneider, and A. Michaelis, "Intercalation Materials for Secondary Batteries Based on Alkali Metal Exchange: Developments and Perspectives," *Journal of Materials Chemistry A* 8 (2020): 16854–16883, https://doi.org/10.1039/D0TA03115A.

19. H. Zhang, C. Li, G. G. Eshetu, et al., "From Solid-Solution Electrodes and the Rocking-Chair Concept to Today's Batteries," *Angewandte Chemie International Edition* 59 (2020): 534–538, https://doi.org/10.1002/anie.201913923.

20. B. Vedhanarayanan, J. Nagaraj, K. Arjunan, and K. C. S. Lakshmi, "Multivalent Metal-Ion Batteries: Unlocking the Future of Post-Lithium Energy Storage," *Nanoenergy Advances* 5 (2025): 13, https://doi.org/10.3390/nanoenergyadv5040013.

21. M. Mahnoor, R. Chandio, A. Inam, and I. U. Ahad, "Critical and Strategic Raw Materials for Energy Storage Devices," *Batteries* 11 (2025): 163, https://doi.org/10.3390/batteries11040163.

22. M. Kamran, M. Raugei, and A. Hutchinson, "Critical Elements for a Successful Energy Transition: A Systematic Review," *Renewable and Sustainable Energy Transition* 4 (2023): 100068, https://doi.org/10.1016/j.rset.2023.100068.

23. D. García-Gusano, D. Iribarren, I. Muñoz, E. Arrizabalaga, L. Mabe, and M. Martín-Gamboa, "The Future Need for Critical Raw Materials Associated with Long-Term Energy and Climate Strategies: The Illustrative Case Study of Power Generation in Spain," *Energy* 314 (2025): 134266, https://doi.org/10.1016/j.energy.2024.134266.

24. F. F., M. M., G. O., F. Q., and F. R., *The Exposure of EU Inventive Efforts to Critical Raw Materials: Evidence From an AI Based Patent Indicator* (European Commission, 2025).

25. J. M. Van Gaalen and J. Chris Slootweg, "From Critical Raw Materials to Circular Raw Materials," *ChemSusChem* 18 (2025): e202401170, https://doi.org/10.1002/cssc.202401170.

26. P. Hegeman and L. Zhou, "Towards a Sustainable Supply of Graphite: A Geological Way Forward," *ES3* 5 (2025): esss2024–014, https://doi.org/10.1144/esss2024-014.

27. S. Fischer, S. Doose, J. Müller, C. Höfels, and A. Kwade, "Impact of Spheroidization of Natural Graphite on Fast-Charging Capability of Anodes for LIB," *Batteries* 9 (2023): 305, https://doi.org/10.3390/batteries9060305.

28. J. Park, S.-J. Cho, S. Shin, R. Kim, D. Shin, and Y. Shin, "Overview of Graphite Supply Chain and Its Challenges," *Geosciences Journal* 29 (2025): 329–341, https://doi.org/10.1007/s12303-025-00027-2.

29. R. Deberdt, N. M. Smith, J. L. Calderon, and S. K. McCall," Critical Minerals Lists for Low-Carbon Transitions: Reviewing Their Structure, Objectives, and Limitations,"*Energy Research & Social Science* 127 (2025): 104252, https://doi.org/10.1016/j.erss.2025.104252.

30. W. Zhang, J. Lu, and Z. Guo, "Challenges and Future Perspectives on Sodium and Potassium Ion Batteries for Grid-Scale Energy Storage," *Materials Today* 50 (2021): 400–417, https://doi.org/10.1016/j.mattod.2021.03.015.

31. M. M. Mashfy, T. A. Alvy, N. Hossain, et al., "Sodium Ion Batteries: A Sustainable Alternative to Lithium-Ion Batteries with an Overview of Market Trends, Recycling, and Battery Chemistry," *Next Energy* 10 (2026): 100478, https://doi.org/10.1016/j.nxener.2025.100478.

32. R. Cancelliere, P. Mele, L. Bartolucci, et al., "Mutual Interaction of Pyrolysis Operating Conditions and Surface Morphology for the Electrochemical Performance of Biochar-Modified Screen-Printed Electrodes," *Journal of Environmental Chemical Engineering* 13 (2025): 115477, https://doi.org/10.1016/j.jece.2025.115477.

33. J. Aslam, M. A. Waseem, X.-M. Lu, W. Sun, and Y. Wang, "From Biochar to Battery Electrodes: A Pathway to Green Lithium and Sodium-Ion Battery Systems," *Chemical Engineering Journal* 505 (2025): 159556, https://doi.org/10.1016/j.cej.2025.159556.

34. Z. Chen, Y. Li, L. Wang, et al., "A Comprehensive Review of Various Carbonaceous Materials for Anodes in Lithium-Ion Batteries," *Dalton Transactions* 53 (2024): 4900–4921, https://doi.org/10.1039/D3DT04010K.

35. G. Zhang, H. Gao, D. Zhang, et al., "Transformative Catalytic Carbon Conversion Enabling Superior Graphitization and Nanopore Engineering in Hard Carbon Anodes for Sodium-Ion Batteries," *Carbon Energy* 7 (2025): e713, https://doi.org/10.1002/cey2.713.

36. M. Bartoli, M. Troiano, P. Giudicianni, et al., "Effect of Heating Rate and Feedstock Nature on Electrical Conductivity of Biochar and Biochar-Based Composites," *Applications in Energy and Combustion Science* 12 (2022): 100089, https://doi.org/10.1016/j.jaecs.2022.100089.

37. X. Deng, F. Teng, M. Chen, et al., "Exploring Negative Emission Potential of Biochar to Achieve Carbon Neutrality Goal in China,"

Nature Communications 15 (2024): 1085, https://doi.org/10.1038/s41467-024-45314-y.

38. K. Zhang, Z. Huang, M. Yang, et al., "Recent Progress in Melt Pyrolysis: Fabrication and Applications of High-Value Carbon Materials From Abundant Sources," *SusMat* 3 (2023): 558–580, https://doi.org/10.1002/sus2.157.

39. M. Devi, S. Rawat, and S. Sharma, "A Comprehensive Review of the Pyrolysis Process: From Carbon Nanomaterial Synthesis to Waste Treatment," *Oxford Open Materials Science* 1 (2020): itab014, https://doi.org/10.1093/oxfmat/itab014.

40. M. Varkolu, S. Gundekari, V. C. S. Palla Omvesh, P. Kumar, S. Bhattacharjee, and T. Vinodkumar, "Recent Advances in Biochar Production, Characterization, and Environmental Applications," *Catalysts* 15 (2025): 243, https://doi.org/10.3390/catal15030243.

41. S. Chandrasekaran, S. Jadhav, S. Mari Selvam, N. Krishnamoorthy, and P. Balasubramanian, "Biochar-Based Materials for Sustainable Energy Applications: A Comprehensive Review," *Journal of Environmental Chemical Engineering* 12 (2024): 114553, https://doi.org/10.1016/j.jece.2024.114553.

42. W.-J. Liu, H. Jiang, and H.-Q. Yu, "Development of Biochar-Based Functional Materials: Toward a Sustainable Platform Carbon Material," *Chemical Reviews* 115 (2015): 12251–12285, https://doi.org/10.1021/acs.chemrev.5b00195.

43. C. R. Correa and A. Kruse, "Biobased Functional Carbon Materials: Production, Characterization, and Applications—A Review," *Materials* 11 (2018): 1568, https://doi.org/10.3390/ma11091568.

44. R. Mori, "Replacing All Petroleum-Based Chemical Products with Natural Biomass-Based Chemical Products: A Tutorial Review," *RSC Sustainability* 1 (2023): 179–212, https://doi.org/10.1039/D2SU00014H.

45. D. Alvira, D. Antorán, M. Vidal, V. Sebastian, and J. J. Manyà, "Vine Shoots-Derived Hard Carbons as Anodes for Sodium-Ion Batteries: Role of Annealing Temperature in Regulating Their Structure and Morphology," *Batteries & Supercaps* 6 (2023): e202300233, https://doi.org/10.1002/batt.202300233.

46. D. Barker-Rothschild, J. Chen, Z. Wan, et al., "Lignin-Based Porous Carbon Adsorbents for CO_2 Capture," *Chemical Society Reviews* 54 (2025): 623–652, https://doi.org/10.1039/D4CS00923A.

47. J. Tu, X. Wang, L. Jiang, et al., "Efficient Graphitization Conversion Strategies of Low-Value Carbonaceous Resources into Advanced Graphitic Carbons," *Chemical Engineering Journal* 505 (2025): 159472, https://doi.org/10.1016/j.cej.2025.159472.

48. S. F. Ahmed, F. Mehejabin, A. A. Chowdhury, et al., "Biochar Produced From Waste-Based Feedstocks: Mechanisms, Affecting Factors, Economy, Utilization, Challenges, and Prospects," *GCB Bioenergy* 16 (2024): e13175, https://doi.org/10.1111/gcbb.13175.

49. A. Schievano, R. Berenguer, A. Goglio, et al., "Electroactive Biochar for Large-Scale Environmental Applications of Microbial Electrochemistry," *ACS Sustainable Chemistry & Engineering* 7 (2019): 18198–18212, https://doi.org/10.1021/acssuschemeng.9b04229.

50. R. Cancelliere, M. Cianciaruso, K. Carbone, and L. Micheli, "Biochar: A Sustainable Alternative in the Development of Electrochemical Printed Platforms," *Chemosensors* 10 (2022): 344, https://doi.org/10.3390/chemosensors10080344.

51. M. M. Hoque, B. K. Saha, A. Scopa, and M. Drosos, "Biochar in Agriculture: A Review on Sources, Production, and Composites Related to Soil Fertility, Crop Productivity, and Environmental Sustainability," *C* 11 (2025): 50, https://doi.org/10.3390/c11030050.

52. Y. Trivedi, M. Sharma, R. K. Mishra, et al., "Biochar Potential for Pollutant Removal during Wastewater Treatment: A Comprehensive Review of Separation Mechanisms, Technological Integration, and Process Analysis," *Desalination* 600 (2025): 118509, https://doi.org/10.1016/j.desal.2024.118509.

53. R. İlay, "Biochar Production From Various Low-Cost Marine Wastes Using Different Production Methods: Characterization of Biochar and Marine Feedstock for Agricultural Purposes," *Marine Pollution Bulletin* 204 (2024): 116623, https://doi.org/10.1016/j.marpolbul.2024.116623.

54. G. Ravindiran, S. Rajamanickam, G. Janardhan, et al., "Production and Modifications of Biochar to Engineered Materials and Its Application for Environmental Sustainability: A Review," *Biochar* 6 (2024): 62, https://doi.org/10.1007/s42773-024-00350-1.

55. P. Prabakar, K. Mustafa Mert, L. Muruganandam, and K. Sivagami, "A Comprehensive Review on Biochar for Electrochemical Energy Storage Applications: An Emerging Sustainable Technology," *Frontiers in Energy Research* 12 (2024): 1448520, https://doi.org/10.3389/fenrg.2024.1448520.

56. Z. Zhang, A. Zhang, S. Wang, J. Sun, L. Hou, and C. Yuan, "Biomass-Derived Hard Carbon with Tunable Microstructures for Sustainable and High-Rate Sodium-Ion Batteries," *New Journal of Chemistry* 49 (2025): 6277–6287, https://doi.org/10.1039/D5NJ00105F.

57. N. Kitchamsetti, K. Kim, H. Han, and S. Mhin, "Biomass-Derived Hard Carbon Anodes for Sodium-Ion Batteries: Recent Advances in Synthesis Strategies," *Nanomaterials* 15 (2025): 1554, https://doi.org/10.3390/nano15201554.

58. J. Górka, C. Vix-Guterl, and C. Matei Ghimbeu, "Recent Progress in Design of Biomass-Derived Hard Carbons for Sodium Ion Batteries," *C* 2 (2016): 24, https://doi.org/10.3390/c2040024.

59. S. Jia, B. Zhang, J. Gao, et al., "Biomass-Derived Hard Carbon Anodes: From Structural Engineering to Industrial Sodium-Ion Battery Applications," *Energy Storage Materials* 80 (2025): 104420, https://doi.org/10.1016/j.ensm.2025.104420.

60. Y. Yang, Z. Liu, Q. Zhang, et al., "Recent Advances of High-Rate Hard Carbon Anodes for Sodium-Ion Batteries: Correlations Between Performance and Microstructure," *Advanced Functional Materials* 36 (2025): e14132, https://doi.org/10.1002/adfm.202514132.

61. M. A. Kabir Hossain, F. Ferdaus, B. A. Johan, A. S. Alzahrani, S. S. Shah, and M. A. Aziz, "Deciphering Sodium Storage in Hard Carbon Anodes: A Review on the Interplay of Microstructure, Interfacial Engineering, and Electrochemical Performance," *Energy & Fuels* 39 (2025): acs.energyfuels.5c04452, https://doi.org/10.1021/acs.energyfuels.5c04452.

62. D. Cai, X. Zhong, L. Xu, et al., "Biomass-Derived Carbon Dots: Synthesis, Modification and Application in Batteries," *Chemical Science* 16 (2025): 4937–4970, https://doi.org/10.1039/D4SC08659G.

63. Q. Zhou, W. Yang, L. Wang, et al., "Biomass Carbon Materials for High-Performance Secondary Battery Electrodes: A Review," *Resources Chemicals and Materials* 3 (2024): 123–145, https://doi.org/10.1016/j.recm.2023.12.002.

64. C. Yuan, H. Xu, S. A. El-khodary, et al., "Recent Advances and Challenges in Biomass-Derived Carbon Materials for Supercapacitors: A Review," *Fuel* 362 (2024): 130795, https://doi.org/10.1016/j.fuel.2023.130795.

65. S. Barbhuiya, B. Bhusan Das, and F. Kanavaris, "Biochar-Concrete: A Comprehensive Review of Properties, Production and Sustainability," *Case Studies in Construction Materials* 20 (2024): e02859, https://doi.org/10.1016/j.cscm.2024.e02859.

66. J. A.I., G. C., L. M.M., et al., "Biomass-Derived Biochar for Electrochemical Energy Storage and Conversion Systems: Opportunities and Challenges," *Future Batteries* 6 (2025): 100077, https://doi.org/10.1016/j.fub.2025.100077.

67. Y. I. Soltan, F. Almomani, M. S. Nasser, and A. S. Bano, "Surface Modification of Biochar for Electrochemical Energy Storage: Focused Mini Review on Supercapacitors and Batteries," *International Journal of Energy Research* 2025 (2025): 5153223, https://doi.org/10.1155/er/5153223.

68. R. Sonawane and B. Kandasubramanian, "Harnessing Functionalized Biochar for Enhanced Electrochemical Properties in Secondary Batteries," *Journal of Electronic Materials* 54 (2025): 5005–5021, https://doi.org/10.1007/s11664-025-12020-4.

69. S. Sobri, and N. I. N. Haris, "Biochar for Energy Storage Applications," Woodhead Publishing Series in *Composites Science and Engineering* 2025 (2025): 159–184, https://doi.org/10.1016/B978-0-443-15403-4.00008-3.

70. C. A. B. Diop, D. Faye, M. Lo, et al., "Engineering Porous Biochar for Electrochemical Energy Storage," *Surfaces* 8 (2025): 87, https://doi.org/10.3390/surfaces8040087.

71. S. S. Senadheera, X. Yuan, B. Yi, S. K. Im, and Y. S. Ok, "Plasma-Modified Biochar for Energy and Environmental Sustainability," *Current Opinion in Chemical Engineering* 49 (2025): 101166, https://doi.org/10.1016/j.coche.2025.101166.

72. S. Simon, P. Harikumar, and P. B. Sreeja, "Green Power: The Role of Plant-Based Biochar in Advanced Energy Storage," *Chemphyschem* 26 (2025): e202400569, https://doi.org/10.1002/cphc.202400569.

73. K. Li, Y. Zhu, H. Cao, et al., "Graphite Made From Coal by High-Temperature Treatment: An Insight into the Nanometric Carbon Structural Evolution," *Minerals* 14 (2024): 1092, https://doi.org/10.3390/min14111092.

74. R. E. Franklin, "Crystallite Growth in Graphitizing and Non-Graphitizing Carbons," *Proceedings of the Royal Society of London Series A* 209 (1951): 196–218, https://doi.org/10.1098/rspa.1951.0197.

75. H. Wendt, and K. Kinoshita, "Carbon, Electrochemical and Physical Properties," *Berichte der Bunsengesellschaft für physikalische Chemie* 198, no. 92 (1988): 1060, https://doi.org/10.1002/bbpc.198800269.

76. D. Nikolis, T. Suthanaruk, K. Amnauypanit, S. Raman, A. B. Burns, and K. Hellgardt, "Comprehensive Characterization of Pyrolytic Carbons From Diverse Methane Pyrolysis Processes: A Comparative Study," *Carbon Trends* 21 (2025): 100583, https://doi.org/10.1016/j.cartre.2025.100583.

77. C. Roiron, A. Cosenza, G. Ferro, J. L. Chen, H. Wang, and P. Atanassov, "Carbon Catalyst Supports for Pt-Based Polymer Electrolyte Membrane Fuel Cells: Porosity, Graphitization, and Chemical Modifications," *Advanced Science* 12 (2025): e08841, https://doi.org/10.1002/advs.202508841.

78. J. R. Dahn, T. Zheng, Y. Liu, and J. S. Xue, "Mechanisms for Lithium Insertion in Carbonaceous Materials," *Science* 270 (1995): 590–593, https://doi.org/10.1126/science.270.5236.590.

79. Q. F. Gillani, B. Bakbolat, B. Tatykayev, F. Sultanov, and A. Mentbayeva, "Biomass-Derived Carbon Materials for Hydrogen Storage: Structure-Performance Relationships and Design Strategies," *Journal of Energy Storage* 135 (2025): 118401, https://doi.org/10.1016/j.est.2025.118401.

80. B. Tratnik, N. Van De Velde, I. Jerman, et al., "Correlating Structural Properties with Electrochemical Behavior of Non-Graphitizable Carbons in Na-Ion Batteries," *Acs Applied Energy Materials* 5 (2022): 10667–10679, https://doi.org/10.1021/acsaem.2c01390.

81. N. Ungureanu, N.-V. Vlăduț, S.-Ș. Biriș, N.-E. Gheorghiță, and M. Ionescu, "Biomass Pyrolysis Pathways for Renewable Energy and Sustainable Resource Recovery: A Critical Review of Processes, Parameters, and Product Valorization," *Sustainability* 17 (2025): 7806, https://doi.org/10.3390/su17177806.

82. D. C. B. D. Santos, R. B. W. Evaristo, R. C. Dutra, P. A. Z. Suarez, E. A. Silveira, and G. F. Ghesti, "Advancing Biochar Applications: A Review of Production Processes, Analytical Methods, Decision Criteria, and Pathways for Scalability and Certification," *Sustainability* 17 (2025): 2685, https://doi.org/10.3390/su17062685.

83. P. T. Do and L. X. Nguyen, "A Review of Thermochemical Decomposition Techniques for Biochar Production," *Environment, Development and Sustainability* (2024), https://doi.org/10.1007/s10668-024-05841-6.

84. K. Sathyabama and S. Firdous, "Effect of Pyrolysis Temperature on the Physicochemical Properties and Structural Characteristics of Agricultural Wastes-Derived Biochar," *ACS Omega* 10 (2025): 37013–37024, https://doi.org/10.1021/acsomega.5c00120.

85. C. Huang, K. Huang, H. Wang, S. Liu, and Y. Zeng, "The Effect of Solid Electrolyte Interface Formation Conditions on the Aging Performance of Li-Ion Cells," *Journal of Solid State Electrochemistry* 15 (2011): 1987–1995, https://doi.org/10.1007/s10008-010-1219-1.

86. B. Liu, Z. Xing, Y. Xue, J. Zhang, and J. Zhai, "Effect of Pyrolysis Temperature on the Carbon Sequestration Capacity of Spent Mushroom Substrate Biochar in the Presence of Mineral Iron," *Molecules* 29 (2024): 5712, https://doi.org/10.3390/molecules29235712.

87. D. Meng, Z. Bian, K. Su, et al., "Improvement of Interphase Stability of Hard Carbon for Sodium-Ion Battery by Ionic Liquid Additives," *Batteries* 11 (2025): 102, https://doi.org/10.3390/batteries11030102.

88. D. Alvira, D. Antorán, and J. J. Manyà, "Plant-Derived Hard Carbon as Anode for Sodium-Ion Batteries: A Comprehensive Review to Guide Interdisciplinary Research," *Chemical Engineering Journal* 447 (2022): 137468, https://doi.org/10.1016/j.cej.2022.137468.

89. S. Watcharamaisakul, N. Janphuang, W. Chueangam, et al., "Synthesis of Turbostratic Graphene Derived From Biomass Waste Using Long Pulse Joule Heating Technique," *Nanomaterials* 15 (2025): 468, https://doi.org/10.3390/nano15060468.

90. P. J. F. Harris, "Non-Graphitizing Carbon: Its Structure and Formation From Organic Precursors," *Eurasian Chemico-Technological Journal* 21 (2019): 227–234, https://doi.org/10.18321/ectj863.

91. M. Ghazinejad, S. Holmberg, O. Pilloni, L. Oropeza-Ramos, and M. Madou, "Graphitizing Non-Graphitizable Carbons by Stress-Induced Routes," *Scientific Reports* 7 (2017): 16551, https://doi.org/10.1038/s41598-017-16424-z.

92. Y. Liu, J. S. Xue, T. Zheng, and J. R. Dahn, "Mechanism of Lithium Insertion in Hard Carbons Prepared by Pyrolysis of Epoxy Resins," *Carbon* 34 (1996): 193–200, https://doi.org/10.1016/0008-6223(96)00177-7.

93. D. A. Stevens and J. R. Dahn, "High Capacity Anode Materials for Rechargeable Sodium-Ion Batteries," *Journal of the Electrochemical Society* 147 (2000): 1271, https://doi.org/10.1149/1.1393348.

94. A. Ge, D. Zhou, K. Inoue, Y. Chen, and S. Ye, "Role of Oxygen in Surface Structures of the Solid-Electrolyte Interphase Investigated by Sum Frequency Generation Vibrational Spectroscopy," *The Journal of Physical Chemistry C* 124 (2020): 17538–17547, https://doi.org/10.1021/acs.jpcc.0c06390.

95. H. Li, X. Lyu, S. Ding, et al., "Study on Product Distribution, Physicochemical Structure Evolution, and Energy Flow in Concentrated Solar Pyrolysis of Walnut Shells," *Fuel Processing Technology* 282 (2026): 108396, https://doi.org/10.1016/j.fuproc.2026.108396.

96. H. C. Ong, K. L. Yu, W.-H. Chen, et al., "Variation of Lignocellulosic Biomass Structure From Torrefaction: A Critical Review," *Renewable and Sustainable Energy Reviews* 152 (2021): 111698, https://doi.org/10.1016/j.rser.2021.111698.

97. S. Rangabhashiyam and P. Balasubramanian, "The Potential of Lignocellulosic Biomass Precursors for Biochar Production: Performance, Mechanism and Wastewater Application—A Review," *Industrial Crops and Products* 128 (2019): 405–423, https://doi.org/10.1016/j.indcrop.2018.11.041.

98. A. Beda, F. Rabuel, M. Morcrette, et al., "Hard Carbon Key Properties Allow for the Achievement of High Coulombic Efficiency and High Volumetric Capacity in Na-Ion Batteries," *Journal of Materials Chemistry A* 9 (2021): 1743–1758, https://doi.org/10.1039/D0TA07687B.

99. H. Shooshtari Gugtapeh, A. H. Aghaii, and A. Simchi, "A Critical Review on the Role of Structural Defects in Electrochemical Nitrate Reduction Catalysts: From Mechanisms to Formation Strategies," *Journal of Environmental Chemical Engineering* 13 (2025): 120221, https://doi.org/10.1016/j.jece.2025.120221.

100. M. Bartoli, A. Piovano, G. A. Elia, et al., "Pristine and Engineered Biochar as Na-Ion Batteries Anode Material: A Comprehensive Overview," *Renewable and Sustainable Energy Reviews* 194 (2024): 114304, https://doi.org/10.1016/j.rser.2024.114304.

101. C. D. M. Saavedra Rios, L. Simonin, A. D. Geyer, C. Matei Ghimbeu, and C. Dupont, "Unraveling the Properties of Biomass-Derived Hard Carbons upon Thermal Treatment for a Practical Application in Na-Ion Batteries," *Energies* 13 (2020): 3513, https://doi.org/10.3390/en13143513.

102. A. Beda, J.-M. Le Meins, P.-L. Taberna, P. Simon, and C. Matei Ghimbeu, "Impact of Biomass Inorganic Impurities on Hard Carbon Properties and Performance in Na-Ion Batteries," *Sustainable Materials and Technologies* 26 (2020): e00227, https://doi.org/10.1016/j.susmat.2020.e00227.

103. N. K. Dayarathne, C. Shi, X. Song, et al., "Unlocking the Potential of Lignin for Sodium-Ion Battery Anodes: From Biorefining to Hard Carbon Engineering," *Energy Storage Materials* 83 (2025): 104705, https://doi.org/10.1016/j.ensm.2025.104705.

104. A. Tomczyk, Z. Sokołowska, and P. Boguta, "Biochar Physicochemical Properties: Pyrolysis Temperature and Feedstock Kind Effects," *Reviews in Environmental Science and Bio/Technology* 19 (2020): 191–215, https://doi.org/10.1007/s11157-020-09523-3.

105. A. Lataf, M. Jozefczak, B. Vandecasteele, et al., "The Effect of Pyrolysis Temperature and Feedstock on Biochar Agronomic Properties," *Journal of Analytical and Applied Pyrolysis* 168 (2022): 105728, https://doi.org/10.1016/j.jaap.2022.105728.

106. X. Wang, X. Yao, J. Sun, et al., "All Biomass-Derived Autogenous Nitrogen-Doped Porous Carbon with Pseudo-Graphitic Structure for Advanced Lithium-Ion Battery Anodes," *Journal of Power Sources* 629 (2025): 235980, https://doi.org/10.1016/j.jpowsour.2024.235980.

107. H. Ge, Z. Xiu, L. Xie, et al., "Modified Conductive Additives Based on Pine Needle-Derived Biomass Carbon for High-Performance Lithium-Ion Batteries," *Biomass and Bioenergy* 200 (2025): 108008, https://doi.org/10.1016/j.biombioe.2025.108008.

108. M. Shi, J. Xiong, S. Xu, et al., "Poria Cocos Waste-Derived Cellulose-Based Biochar as an Advanced Porous Anode Material for Lithium-Ion Batteries," *Journal of Materials Chemistry C* 13 (2025): 19330–19339, https://doi.org/10.1039/D5TC01814E.

109. M. J. Barbosa Nogueira, S. Chauque, V. Sperati, et al., "Untreated Bamboo Biochar as Anode Material for Sustainable Lithium Ion Batteries," *Biomass and Bioenergy* 193 (2025): 107511, https://doi.org/10.1016/j.biombioe.2024.107511.

110. M. Y. Perdana, V. Shukla, I. J. Gusthigngnawadu, and P. A. Johnson, "Pre-Lithiated Soft-Carbon Derived From Biochar for Lithium-Ion Batteries," *Meeting Abstracts* MA2025-02 (2025): 595–595, https://doi.org/10.1149/MA2025-023595mtgabs.

111. R. C. F. Silva, R. L. D. F. Filho, K. S. D. Santos, et al., "Effect of CO2 Activation on Ordered Mesoporous Carbons Obtained From Tannin Biomass for Cathode Support on Stable Lithium-Sulfur Batteries," *Materials Today Communications* 47 (2025): 113108, https://doi.org/10.1016/j.mtcomm.2025.113108.

112. Z. Zhang, J. Yang, P. Lv, et al., "A High Electrochemical Performance Biochar-Based Cathode Material Derived From Antibiotic Bacteria Residues with Layered Porous Structure," *Biomass and Bioenergy* 193 (2025): 107559, https://doi.org/10.1016/j.biombioe.2024.107559.

113. D. Bhatia and A. K. Saroha, "Rice Straw-Derived Biochar as Anode Material for Lithium-Ion Battery: A Step toward Sustainable Development," *Energy Technology* 12 (2024): 2400096, https://doi.org/10.1002/ente.202400096.

114. Z. Shi, Y. Jin, T. Han, et al., "Bio-Based Anode Material Production for Lithium–ion Batteries through Catalytic Graphitization of Biochar: The Deployment of Hybrid Catalysts," *Scientific Reports* 14 (2024): 3966, https://doi.org/10.1038/s41598-024-54509-8.

115. C. Zhai, P. He, Y. He, et al., "Urchin Flower-Like SnO2 Nanosheets Anchored on Waste Biomass Carbon as Advanced Anode for Lithium-Ion Batteries," *Ceramics International* 50 (2024): 3546–3555, https://doi.org/10.1016/j.ceramint.2023.11.103.

116. T. M. W. J. Bandara, A. M. B. S. Alahakoon, B.-E. Mellander, and I. Albinsson, "Activated Carbon Synthesized From Jack Wood Biochar for High Performing Biomass Derived Composite Double Layer Supercapacitors," *Carbon Trends* 15 (2024): 100359, https://doi.org/10.1016/j.cartre.2024.100359.

117. I. Alouiz, M. Benhadj, E. Dahmane, M. Sennoune, M.-Y. Amarouch, and D. Mazouzi, "Elaboration of Fibrous Structured Activated Carbon From Olive Pomace via Chemical Activation and Low-Temperature Pyrolysis," *Heliyon* 10 (2024): e38886, https://doi.org/10.1016/j.heliyon.2024.e38886.

118. S. Khasim, S. G. Dastager, M. I. Alahmdi, et al., "Green Synthesis of Multifunctional Cu/MnO@Biochar 3D Structure as a High-Performance Anode Material in Li-Ion Batteries and Oxidative Removal of Cango-Red Dye," *Case Studies in Chemical and Environmental Engineering* 9 (2024): 100561, https://doi.org/10.1016/j.cscee.2023.100561.

119. Q. Wu, X. Dou, F. Liu, et al., "Hierarchical Porous Biomass-Derived Electrodes with High Areal Loading for Lithium–sulfur Batteries," *Rsc Advances* 15 (2025): 17746–17754, https://doi.org/10.1039/D5RA02380G.

120. J. Sang, C. Sun, J. Pan, et al., "Seaweed═Modification of Si by Natural Nitrogen-Doped Porous Biochar for High-Efficiency Lithium Batteries," *Acs Applied Materials & Interfaces* 16 (2024): 11389–11399, https://doi.org/10.1021/acsami.3c15459.

121. M. He, J. Zhao, D. Wang, et al., "Microwave-Assisted Catalytic Pyrolysis of Biomass with Biochar Materials Derived From Spent Lithium-Ion Batteries: Microwave Absorption and Pyrolysis Characteristics," *Journal of Environmental Chemical Engineering* 12 (2024): 112099, https://doi.org/10.1016/j.jece.2024.112099.

122. I. Tunc, B. D. Karahan, and O. Keles, "Biomass-Derived SiOx/C Nanocomposite Anode Synthesis by Induction Heating for Lithium Ion Battery," *Applied Physics A* 130 (2024): 677, https://doi.org/10.1007/s00339-024-07841-9.

123. Q. Sun, X. Cheng, C. Ma, J. Wang, W. Qiao, and L. Ling, "NiSe Nanoparticles Decorated Corn Stalk Derived 2D Carbon Nanosheet as Separator Modifier for High-Performance Lithium-Sulfur Batteries," *Journal of Power Sources* 585 (2023): 233645, https://doi.org/10.1016/j.jpowsour.2023.233645.

124. A. A. Belmesov, A. A. Glukhov, R. R. Kayumov, et al., "Using Aquatic Plant-Derived Biochars as Carbon Materials for the Negative Electrodes of Li-Ion Batteries," *Coatings* 13 (2023): 2075, https://doi.org/10.3390/coatings13122075.

125. M.-M. Titirici, R. J. White, C. Falco, and M. Sevilla, "Black Perspectives for a Green Future: Hydrothermal Carbons for Environment Protection and Energy Storage," *Energy & Environmental Science* 5 (2012): 6796–6822, https://doi.org/10.1039/C2EE21166A.

126. D. A. Stevens and J. R. Dahn, "The Mechanisms of Lithium and Sodium Insertion in Carbon Materials," *Journal of the Electrochemical Society* 148 (2001): A803, https://doi.org/10.1149/1.1379565.

127. L.-F. Zhao, Z. Hu, W.-H. Lai, et al., "Hard Carbon Anodes: Fundamental Understanding and Commercial Perspectives for Na-Ion Batteries beyond Li-Ion and K-Ion Counterparts," *Advanced Energy Materials* 11 (2021): 2002704, https://doi.org/10.1002/aenm.202002704.

128. W. Zhang, J. Mao, S. Li, Z. Chen, and Z. Guo, "Phosphorus-Based Alloy Materials for Advanced Potassium-Ion Battery Anode," *Journal of the American Chemical Society* 139 (2017): 3316–3319, https://doi.org/10.1021/jacs.6b12185.

129. C. Bommier and X. Ji, "Recent Development on Anodes for Na-Ion Batteries," *Israel Journal of Chemistry* 55 (2015): 486–507, https://doi.org/10.1002/ijch.201400118.

130. A. O. Orilonise, K. O. Iwuozor, E. C. Emenike, J. Emeghai, and A. G. Adeniyi, "Waste-Derived Carbon Materials for High-Efficiency Lithium-Ion Batteries: A Review," *Environmental Surfaces and Interfaces* 4 (2026): 98–112, https://doi.org/10.1016/j.esi.2026.01.001.

131. D. P. DiVincenzo and E. J. Mele, "Cohesion and Structure in Stage-1 Graphite Intercalation Compounds," *Physical Review. B* 32 (1985): 2538–2553, https://doi.org/10.1103/PhysRevB.32.2538.

132. O. Lenchuk, P. Adelhelm, and D. Mollenhauer, "New Insights into the Origin of Unstable Sodium Graphite Intercalation Compounds," *Physical Chemistry Chemical Physics* 21 (2019): 19378–19390, https://doi.org/10.1039/C9CP03453F.

133. Y. Cao, L. Xiao, M. L. Sushko, et al., "Sodium Ion Insertion in Hollow Carbon Nanowires for Battery Applications," *Nano Letters* 12 (2012): 3783–3787, https://doi.org/10.1021/nl3016957.

134. C. Bommier, T. W. Surta, M. Dolgos, and X. Ji, "New Mechanistic Insights on Na-Ion Storage in Nongraphitizable Carbon," *Nano Letters* 15 (2015): 5888–5892, https://doi.org/10.1021/acs.nanolett.5b01969.

135. S. Alvin, D. Yoon, C. Chandra, et al., "Revealing Sodium Ion Storage Mechanism in Hard Carbon," *Carbon* 145 (2019): 67–81, https://doi.org/10.1016/j.carbon.2018.12.112.

136. N. Sun, Z. Guan, Y. Liu, et al., "Extended "Adsorption–Insertion" Model: A New Insight into the Sodium Storage Mechanism of Hard Carbons," *Advanced Energy Materials* 9 (2019): 1901351, https://doi.org/10.1002/aenm.201901351.

137. X. Chen, C. Liu, Y. Fang, et al., "Understanding of the Sodium Storage Mechanism in Hard Carbon Anodes," *Carbon Energy* 4 (2022): 1133–1150, https://doi.org/10.1002/cey2.196.

138. C. Wu, Y. Yang, Y. Zhang, et al., "Hard Carbon for Sodium-Ion Batteries: Progress, Strategies and Future Perspective," *Chemical Science* 15 (2024): 6244–6268, https://doi.org/10.1039/D4SC00734D.

139. K. Zhao, Y. Xin, Q. Zhou, et al., "Oxygen Functionalities Incorporation into Hard Carbon Anodes for High Rate Sodium Ion Storage," *Journal of Power Sources* 657 (2025): 238171, https://doi.org/10.1016/j.jpowsour.2025.238171.

140. T. Zhang, T. Zhang, F. Wang, and F. Ran, "High-Efficiently Doping Nitrogen in Kapok Fiber-Derived Hard Carbon Used as Anode Materials for Boosting Rate Performance of Sodium-Ion Batteries," *Journal of Energy Chemistry* 96 (2024): 472–482, https://doi.org/10.1016/j.jechem.2024.05.005.

141. M. Yanilmaz, B. Temel, E. Bayram, M. Tosun, I. Topcu, and J. Kim, "Sustainable Biowaste Conversion into Microporous Carbons for Efficient Energy Storage Solutions in Sodium-Ion Batteries," *Journal of Environmental Chemical Engineering* 13 (2025): 118559, https://doi.org/10.1016/j.jece.2025.118559.

142. Q. Wu, K. Shu, L. Zhao, and J. Zhang, "Pomegranate Peel-Derived Hard Carbons as Anode Materials for Sodium-Ion Batteries," *Molecules* 29 (2024): 4639, https://doi.org/10.3390/molecules29194639.

143. G. Shen, B. Li, Y. Xu, et al., "Waste Biomass Garlic Stem-Derived Porous Carbon Materials as High-Capacity and Long-Cycling Anode for Lithium/Sodium-Ion Batteries," *Journal of Colloid and Interface Science* 653 Pt B (2023): 1588–1599, https://doi.org/10.1016/j.jcis.2023.09.150.

144. N. J. Song, Guo, C. Ma, Y. Zhao, W. Li, and B. Li, "Modulating the Graphitic Domains and Pore Structure of Corncob-Derived Hard Carbons by Pyrolysis to Improve Sodium Storage," *Molecules* 28 (2023): 3595, https://doi.org/10.3390/molecules28083595.

145. I. Alouiz, M. Aqil, A. Chari, M. Dahbi, M. Amarouch, and D. Mazouzi, "Influence of Phosphorus Activation and Carbonization Temperature on the Electrochemical Performance of Hard Carbon Made From Olive Pomace as an Anode for Sodium-Ion Batteries," *RSC Advances* 15 (2025): 19546–19560, https://doi.org/10.1039/d5ra02547h.

146. Y. Rao, O. Sundman, M. Holmboe, N. Tavajohi, and C. Ohlin, "Scotch Pine Cones-Derived Hard Carbon as an Anode Material for Sodium-Ion Battery Applications," *ACS Omega* 10 (2025): 11158–11167, https://doi.org/10.1021/acsomega.4c10363.

147. X. Zhang, Y. Cao, G. Li, et al., "Exploring Carbonization Temperature to Create Closed Pores for Hard Carbon as High-Performance Sodium-Ion Battery Anodes," *Small* 20 (2024): 2311197, https://doi.org/10.1002/smll.202311197.

148. D. P. N. Nahda, A. R. Sanjaya, F. Rahmawati, et al., "Synthesis of Mesoporous Carbon From Banana Peels with Silica gel 60 as the Hard Templates," *Rsc Advances* 15 (2025): 4536–4545, https://doi.org/10.1039/D4RA08322A.

149. X. Sun, X. Gao, Z. Li, et al., "Nanowires Framework Supported Porous Lotus-Carbon Anode Boosts Lithium-Ion and Sodium-Ion Batteries," *Small Methods* 8 (2024): 2300746, https://doi.org/10.1002/smtd.202300746.

150. X. He, L. Li, X. Wu, and S. Chou, "Sustainable Hard Carbon for Sodium-Ion Batteries: Precursor Design and Scalable Production Roadmaps," *Advanced Materials* 37 (2025): 2506066, https://doi.org/10.1002/adma.202506066.

151. Q. Wang, L. Du, S. Wang, L. Yu, X. Tu, and H. Zhang, "Biomass-Derived Hard Carbon Anodes Processed with Deep Eutectic Solvents for High-Performance Sodium-Ion Batteries," *ACS Omega* 10 (2025): 23620–23628, https://doi.org/10.1021/acsomega.5c02496.

152. Y. Li, D. Xia, L. Tao, et al., "Hydrothermally Assisted Conversion of Switchgrass into Hard Carbon as Anode Materials for Sodium-Ion Batteries," *ACS Applied Materials & Interfaces* 16 (2024): 28461–28472, https://doi.org/10.1021/acsami.4c02734.

153. J. Huang, L. Liu, Q. Fan, S. Li, H. Cui, and J. Xu, "Nitrogen-Doped Hard Carbon Anode From Redwood Biomass for Sodium-Ion Batteries with High Initial Coulombic Efficiency and Enhanced Rate Capability," *Small* 21 (2025): 202505579, https://doi.org/10.1002/smll.202505579.

154. Y. Luo, Y. Xu, X. Li, K. Zhang, Q. Pang, and A. Qin, "Boosting the Initial Coulomb Efficiency of Sisal Fiber-Derived Carbon Anode for Sodium Ion Batteries by Microstructure Controlling," *Nanomaterials* 13 (2023): 881, https://doi.org/10.3390/nano13050881.

155. N. Nieto, J. Porte, D. Saurel, et al., "Use of Hydrothermal Carbonization to Improve the Performance of Biowaste-Derived Hard Carbons in Sodium Ion-Batteries," *ChemSusChem* 16 (2023): e202301053, https://doi.org/10.1002/cssc.202301053.

156. W. Li, J. Li, B. W. Biney, et al., "Innovative Synthesis and Sodium Storage Enhancement of Closed-Pore Hard Carbon for Sodium-Ion Batteries," *Energy Storage Materials* 74 (2025): 103867, https://doi.org/10.1016/j.ensm.2024.103867.

157. D. Antorán, D. Alvira, M. E. Peker, et al., "Waste Hemp Hurd as a Sustainable Precursor for Affordable and High-Rate Hard Carbon-Based Anodes in Sodium-Ion Batteries," *Energy & Fuels* 37 (2023): 9650–9661, https://doi.org/10.1021/acs.energyfuels.3c01040.

158. W. Zhang, M. Li, Y. Chen, and Z. Zhang, "Facile Synthesis of Honeycomb-Structured Biochar with High Specific Surface and Its Electrochemical Properties as Anodes for Na-Ion Batteries," *Ionics* 29 (2023): 5195–5203, https://doi.org/10.1007/s11581-023-05235-0.

159. M. Ali, M. Khan, F. Mahmood, et al., "Porous Biochar Synthesized From Pine Sawdust via Molten Salt Pyrolysis/Activation for Advanced

Li/Na-Selenium Batteries," *Materials Today Communications* 46 (2025): 112743, https://doi.org/10.1016/j.mtcomm.2025.112743.

160. G. S. dos Reis, C. M. Subramaniyam, A. Grimm, et al., "Biomass-Derived Macroporous Carbon–tin Oxide Composites as Stable and High-Capacity Anodes for Lithium-Ion and Sodium-Ion Batteries: Experimental Study and GFN1-xTB Calculations," *Physical Chemistry Chemical Physics* 27 (2025): 14000–14014, https://doi.org/10.1039/D5CP01053E.

161. A. Patel, R. Mishra, R. K. Tiwari, et al., "Sustainable and Efficient Energy Storage: A Sodium Ion Battery Anode From *Aegle marmelos* Shell Biowaste," *Journal of Energy Storage* 72 (2023): 108424, https://doi.org/10.1016/j.est.2023.108424.

162. G. Wu, H. Zhang, X. Zhang, et al., "Converting Biomass Tar into N-Doped Biochar: A Promising Anode Material for Enhanced Sodium-Ion Batteries," *Journal of Analytical and Applied Pyrolysis* 188 (2025): 107051, https://doi.org/10.1016/j.jaap.2025.107051.

163. B. Lu, J.-X. Song, D.-R. Deng, et al., "Self-Doped Porous Sorghum Husk-Derived Carbon as Anode for High Performance Sodium-Ion Batteries at Low Temperatures," *Journal of Energy Storage* 102 (2024): 114056, https://doi.org/10.1016/j.est.2024.114056.

164. S.-J. Jiang, Y.-S. Xu, X.-W. Sun, et al., "Lignocellulolytic Bacterial Engineering for Tailoring the Microstructure of Hard Carbon as a Sodium-Ion Battery Anode with Fast Plateau Kinetics," *Journal of the American Chemical Society* 147 (2025): 8088–8092, https://doi.org/10.1021/jacs.4c15593.

165. R. Duan, X. Zhang, T. Zheng, et al., "Discarded Sulfuric Acid Paper-Derived Hard Carbon as High-Performance Anode Material for Sodium-Ion Batteries," *Journal of Energy Storage* 100 (2024): 113563, https://doi.org/10.1016/j.est.2024.113563.

166. R. Liang, Y. Feng, Z. Tong, D. Xiong, and M. He, "Hard Carbon Microtubes Made From Metaplexis Japonica Seed Hair Fibers as High-Performance Anode Material for Sodium-Ion Batteries," *Langmuir* 41 (2025): 22592–22600, https://doi.org/10.1021/acs.langmuir.5c03219.

167. A. M. Escamilla-Pérez, A. Beda, L. Simonin, M.-L. Grapotte, J. M. Le-Meins, and C. Matei Ghimbeu, "Biopolymer-Based Hard Carbons: Correlations between Properties and Performance as a Na-Ion Battery Anode," *Acs Applied Energy Materials* 6 (2023): 7419–7432, https://doi.org/10.1021/acsaem.3c00640.

168. J. Huo, C. Li, P. Xia, N. Fan, W. Mao, and K. Bao, "Preparation of Hard Carbon From Acid-Treated Locust Wood as Anode Material for Sodium-Ion Batteries," *Journal of Applied Electrochemistry* 55 (2025): 1099–1110, https://doi.org/10.1007/s10800-024-02235-4.

169. S. Komaba, T. Hasegawa, M. Dahbi, and K. Kubota, "Potassium Intercalation into Graphite to Realize High-Voltage/High-Power Potassium-Ion Batteries and Potassium-Ion Capacitors," *Electrochemistry Communications* 60 (2015): 172–175, https://doi.org/10.1016/j.elecom.2015.09.002.

170. W. Luo, J. Wan, B. Ozdemir, et al., "Potassium Ion Batteries with Graphitic Materials," *Nano Letters* 15 (2015): 7671–7677, https://doi.org/10.1021/acs.nanolett.5b03667.

171. Z. Jian, W. Luo, and X. Ji, "Carbon Electrodes for K-Ion Batteries," *Journal of the American Chemical Society* 137 (2015): 11566–11569, https://doi.org/10.1021/jacs.5b06809.

172. T. Hosaka, K. Kubota, A. S. Hameed, and S. Komaba, "Research Development on K-Ion Batteries," *Chemical Reviews* 120 (2020): 6358–6466, https://doi.org/10.1021/acs.chemrev.9b00463.

173. R. Rajagopalan, Y. Tang, X. Ji, C. Jia, and H. Wang, "Advancements and Challenges in Potassium Ion Batteries: A Comprehensive Review," *Advanced Functional Materials* 30 (2020): 1909486, https://doi.org/10.1002/adfm.201909486.

174. N. Khan, G. Han, and S. A. Mazari, "Carbon Nanotubes-Based Anode Materials for Potassium Ion Batteries: A Review," *Journal of Electroanalytical Chemistry* 907 (2022): 116051, https://doi.org/10.1016/j.jelechem.2022.116051.

175. L. Larbi, B. Larhrib, L. Madec, C. Vaulot, L. Monconduit, and C. Matei Ghimbeu, "Impact of Milling Conditions on Hard and Soft Carbon Properties and Performance in Potassium-Ion Batteries," *Acs Applied Energy Materials* 7 (2024): 3378–3392, https://doi.org/10.1021/acsaem.4c00148.

176. S. Chen, K. Tang, F. Song, et al., "Porous Hard Carbon Spheres Derived From Biomass for High-Performance Sodium/Potassium-Ion Batteries," *Nanotechnology* 33 (2021): 055401, https://doi.org/10.1088/1361-6528/ac317d.

177. M. Cai, H. Zhang, Y. Zhang, et al., "Boosting the Potassium-Ion Storage Performance Enabled by Engineering of Hierarchical MoSSe Nanosheets Modified with Carbon on Porous Carbon Sphere," *Science Bulletin* 67 (2022): 933–945, https://doi.org/10.1016/j.scib.2022.02.007.

178. L. Rui, A. Keyu, O. Hao, et al., "Ferroelectricity Enhances Ion Migration in Hard Carbon Anodes for High-Performance Potassium Ion Batteries," *Nanoscale* 17 (2025): 5981, https://doi.org/10.1039/d4nr04916k.

179. S. Jung, J. Min, H. Choi, et al., "Role of Mesoporosity in Hard Carbon Anodes for High-Energy and Stable Potassium-Ion Storage," *Small* 21 (2025): 2410232, https://doi.org/10.1002/smll.202410232.

180. M. Piernas-Muñoz and M. Zarrabeitia, "Revisiting Intercalation Anode Materials for Potassium-Ion Batteries," *Materials* 18 (2025): 190, https://doi.org/10.3390/ma18010190.

181. Y. Wang, J. Zeng, Y. Wang, et al., "Biomass-Derived Carbon With Large Interlayer Spacing for Anode of Potassium Ion Batteries," *Advanced Materials* 36 (2024): 2410132, https://doi.org/10.1002/adma.202410132.

182. J. Wang, J. Yuan, L. Bai, et al., "Doped Hard Carbon Nanotube Bundles for Superior Potassium Storage," *Acs Applied Nano Materials* 8 (2025): 13332–13339, https://doi.org/10.1021/acsanm.5c01850.

183. Y. Liang, S. Xu, Z. Lu, et al., "Revealing the Potassium Storage Mechanism of Cross-Linked Hybridization Soft-Hard Carbon Anode Materials for Potassium-Ion Batteries," *Journal of Energy Storage* 126 (2025): 117103, https://doi.org/10.1016/j.est.2025.117103.

184. C. Li, Y. Zhu, S. Li, X. Liu, and Q. Xiong, "Bark-Derived Oxygen-Doped Porous Hard Carbon Anodes for Potassium-Ion Batteries," *Energy Technology* 13 (2025): 2402287, https://doi.org/10.1002/ente.202402287.

185. C. Fu, F. Hua, H. Huang, et al., "High-Capacity and Durable Enabled by Modulation of Nitrogen Doping and Graphite Nanodomains in, *Calophyllum inophyllum*, L. Derived Hard Carbon Anode for Potassium Storage," *Journal of Power Sources* 659 (2025): 238392, https://doi.org/10.1016/j.jpowsour.2025.238392.

186. X. Chang, H. Chen, C. Gao, et al., "Starch-Assisted Microcrystalline Regulation of Coal-Derived Carbon for High-Performance Potassium Ion Batteries," *Journal of Materials Science & Technology* 250 (2026): 53–61, https://doi.org/10.1016/j.jmst.2025.05.070.

187. J. L. Gómez-Urbano, C. Leibing, M. Jauregui, et al.,"Unravelling Charge Storage Mechanisms of Lithium, Sodium and Potassium into Graphene-Coffee Waste Derived Hard Carbon Composites," *Batteries & Supercaps* 6 (2023): e202200508, https://doi.org/10.1002/batt.202200508.

188. M. Kim, L. Ma, Z. Li, et al., "N and S Co-Doped Nanosheet-Like Porous Carbon Derived From Sorghum Biomass: Mechanical Nanoarchitecturing for Upgraded Potassium Ion Batteries," *Journal of Materials Chemistry A* 11 (2023): 16626–16635, https://doi.org/10.1039/D3TA03215A.

189. N. P. N. Puneeth, K. Rajkumar, A. Soundarya, et al., "Nano-Graphitic Crystallites Effect on the Improved K-Ion Intercalation Properties of *Kigelia Africana* Fruit-Derived Hard Carbon for Potassium-Ion Batteries," *Chemical Engineering Journal* 480 (2024): 147835, https://doi.org/10.1016/j.cej.2023.147835.

190. Y. Zhu, S. Li, C. Li, et al., "Synthesizing Hard Carbon Anodes for Potassium-Ion Batteries From Black Liquor and Deinking Sludge," *Fuel* 371 (2024): 131956, https://doi.org/10.1016/j.fuel.2024.131956.

191. J. Chen, L. Tan, C. Lin, et al., "Graphite-Catalyzed Carbonization of Biowaste Unlocks Energy-Dense, High-Rate, and Long-Lifespan Potassium-Ion Batteries," *Chemical Engineering Journal* 515 (2025): 163832, https://doi.org/10.1016/j.cej.2025.163832.

192. L. Wang, Z. Lu, S. Xu, et al., "Constructing Hard Carbon Submicron Spheres with Boron Doping as Advanced Anode Materials toward Enhanced Sodium and Potassium-Ion Storage," *Acs Applied Energy Materials* 8 (2025): 10321–10333, https://doi.org/10.1021/acsaem.5c01173.

193. L. Tan, J. Chen, L. Wang, et al., "High-Coulombic-Efficiency Hard Carbon Anode Material for Practical Potassium-Ion Batteries,"*Batteries & Supercaps* 7 (2024): e202400010, https://doi.org/10.1002/batt.202400010.

194. Z. Pang, L. Wang, S. Wan, et al., "Wedelia Chinensis-Derived Biomass Porous Carbon as Anode Material for High Performance Sodium/Potassium-Ion Batteries," *Ionics* 30 (2024): 4655–4664, https://doi.org/10.1007/s11581-024-05604-3.

195. R. Sahoo, B. Tharigopala Vincent, L. Thirugnamam, S. Venkatachalam, and R. Sundara, "Effect of Addition of Thermally Annealed Graphene in Tender Coconut-Derived Hard Carbon for Potassium Ion Battery," *Acs Applied Energy Materials* 7 (2024): 7006–7018, https://doi.org/10.1021/acsaem.4c01231.

196. K. Li, C. Fan, H. Xu, et al., "Fe2O3 Nanoparticles Anchored on N-Doped Pinecone-Based Porous Carbon as Potential Anode for Potassium-Ion Battery," *Journal of Physics and Chemistry of Solids* 192 (2024): 112091, https://doi.org/10.1016/j.jpcs.2024.112091.

197. H. Ou, B. Pei, Y. Zhou, et al., "From Natural Fibers to High-Performance Anodes: Sisal Hemp Derived Hard Carbon for Na-/K-Ion Batteries and Mechanism Exploration," *Small Methods* 9 (2025): 2400839, https://doi.org/10.1002/smtd.202400839.

198. Q. Pan, B. Li, S. Liu, et al., "Flower-Like Graphitic Carbon Derived From Biomass for Anode of Potassium Ion Battery," *Chemical Engineering Science* 304 (2025): 121043, https://doi.org/10.1016/j.ces.2024.121043.

199. J. Hao, M. Ye, A. P. Vijaya Kumar Saroja, et al., "Platanus Occidentalis L. Fruit-Derived Carbon Materials for Electrochemical Potassium Storage," *Nanotechnology* 36 (2025): 125701, https://doi.org/10.1088/1361-6528/ada8b4.

200. J. Song, S. Jiang, Y. Wang, et al., "Synergistic Effects of P-Functionalization and Localized Graphitization in Sustainable Hard Carbon for Enhanced Sodium and Potassium Storage," *Journal of Colloid and Interface Science* 686 (2025): 1200–1214, https://doi.org/10.1016/j.jcis.2025.02.028.

201. T. Sun, C. Gao, X. Tan, et al., "High-Value Utilization of Corn Plants Derived Biomass Carbon Materials for Potassium Ion Storage," *Sustainable Materials and Technologies* 44 (2025): e01359, https://doi.org/10.1016/j.susmat.2025.e01359.

202. T. Zhu, B. Mai, P. Hu, et al., "Bagasse-Derived Hard Carbon Anode with an Adsorption–Intercalation Mechanism for High-Rate Potassium Storage," *Acs Applied Energy Materials* 6 (2023): 2370–2377, https://doi.org/10.1021/acsaem.2c03628.

203. Y. Zhang, D. Qi, Y. Wang, et al., "Rhus Typhina Wood-Based Biochar Electrodes for High Effective Potassium Storage Capacity," *Journal of Materials Science: Materials in Electronics* 35 (2024): 2136, https://doi.org/10.1007/s10854-024-13890-w.

204. R. D. Shannon, "Revised Effective Ionic Radii and Systematic Studies of Interatomic Distances in Halides and Chalcogenides," *Acta Crystallographica Section A* 32 (1976): 751–767, https://doi.org/10.1107/S0567739476001551.

205. N. Nitta, F. Wu, J. T. Lee, and G. Yushin, "Li-Ion Battery Materials: Present and Future," *Materials Today* 18 (2015): 252–264, https://doi.org/10.1016/j.mattod.2014.10.040.

206. C. Yang, X. Zhang, J. Li, et al., "Holey Graphite: A Promising Anode Material with Ultrahigh Storage for Lithium-Ion Battery," *Electrochimica Acta* 346 (2020): 136244, https://doi.org/10.1016/j.electacta.2020.136244.

207. W. Duan, S. Chen, X. Zhuang, N. Jiang, and Y. Li, "Anode Materials for Sodium-Ion Batteries: Current Status and Future Perspectives," *Journal of Power Sources* 666 (2026): 239163, https://doi.org/10.1016/j.jpowsour.2025.239163.

208. S. Tan, Y. Wen, J. Li, et al., "Fast-Charging Capabilities of Hard Carbon Anodes in Sodium-Ion Batteries: Mechanisms, Strategies, and Prospects," *Carbon Neutralization* 4 (2025): e70071, https://doi.org/10.1002/cnl2.70071.

209. Y. Chen, B. Xi, M. Huang, et al., "Defect-Selectivity and "Order-in-Disorder" Engineering in Carbon for Durable and Fast Potassium Storage," *Advanced Materials* 34 (2022): 2108621, https://doi.org/10.1002/adma.202108621.

210. W. Li, M. Zhou, H. Li, K. Wang, S. Cheng, and K. Jiang, "A High Performance Sulfur-Doped Disordered Carbon Anode for Sodium Ion Batteries," *Energy & Environmental Science* 8 (2015): 2916–2921, https://doi.org/10.1039/C5EE01985K.

211. V. C. A. Ficca, M. Sbroscia, E. Stellino, et al., "Non-Chemical Route to PGM-Free via N+ Ion Implantation in Vertically Aligned Carbon Nanotubes," *Advanced Functional Materials* 35 (2025): 2413308, https://doi.org/10.1002/adfm.202413308.

212. S. Liu, Q. Zhang, J. Liu, et al., "Nitrogen-Doped Porous Carbons Derived From Peanut Shells as Efficient Electrodes for High-Performance Supercapacitors," *International Journal of Molecular Sciences* 25 (2024): 7583, https://doi.org/10.3390/ijms25147583.

213. N. Li, H. Li, and H. Huang, "Synergistic Nitrogen-Doping and Defect Engineering in Hard Carbon: Unlocking Ultrahigh Rate Capability and Long-Cycling Stability for Sodium-Ion Battery Anodes," *Materials* 18 (2025): 2397, https://doi.org/10.3390/ma18102397.

214. M. Li, Z. Li, F. Bai, H. Woo, Z. Osman, and B. Fei, "Multitrack Boosted Hard Carbon Anodes: Innovative Paths and Advanced Performances in Sodium-Ion Batteries," *Small* 21 (2025): 2500645, https://doi.org/10.1002/smll.202500645.

215. K. Pongpanyanate, S. Roddecha, C. Piyanirund, T. Phraewphiphat, and P. Hasin, "Dispersed MnO2 Nanoparticles/Sugarcane Bagasse-Derived Carbon Composite as an Anode Material for Lithium-Ion Batteries," *RSC Advances* 14 (2024): 2354–2368, https://doi.org/10.1039/d3ra04008a.

216. Z. Liu, J. Zhao, H. Yao, et al., "P-Doped Spherical Hard Carbon with High Initial Coulombic Efficiency and Enhanced Capacity for Sodium Ion Batteries," *Chemical Science* 15 (2024): 8478–8487, https://doi.org/10.1039/d4sc01395f.

217. W. Li, X. Lu, B. Biney, J. Li, Y. Yan, and K. Chen, "In-Situ Synthesis of Heteroatom-Doped Hard Carbon for Sodium-Ion Batteries: Dual Benefits for Green Energy and Environment," *Journal of Colloid and Interface Science* 677 Pt B (2024): 312–322, https://doi.org/10.1016/j.jcis.2024.07.248.

218. J. Lan, Q. Lin, X. Li, et al., "Tailoring the Biochar Microstructure to Increase Closed Nanopores in Biomass-Derived Hard Carbons for Boosting Sodium-Ion Storage," *Carbon* 249 (2026): 121220, https://doi.org/10.1016/j.carbon.2025.121220.

219. Z. Li, C. Bommier, Z. S. Chong, et al., "Mechanism of Na-Ion Storage in Hard Carbon Anodes Revealed by Heteroatom Doping," *Advanced Energy Materials* 7 (2017): 1602894, https://doi.org/10.1002/aenm.201602894.

220. J. Li, K. V. Mejía-Centeno, M. D. Khan, et al., "Beyond Imperfect Match: Silicon/Graphite Hybrid Anodes for High-Energy–Density Lithium-Ion Batteries," *Advanced Energy Materials* 16 (2026): e05674, https://doi.org/10.1002/aenm.202505674.

221. J. Li, N. Sawut, Y. Zhao, P. Liu, Y. Wang, and Y. Cao, "Microstructure-Mechanism-Performance Relationships in Hard Carbon Anode Materials for Sodium-Ion Batteries," *New Carbon Materials* 40 (2025): 860–868, https://doi.org/10.1016/S1872-5805(25)61023-7.

222. F. Yuan, Z. Li, D. Zhang, et al., "Fundamental Understanding and Research Progress on the Interfacial Behaviors for Potassium-Ion Battery Anode," *Advanced Science* 9 (2022): 2200683, https://doi.org/10.1002/advs.202200683.

223. Y. Zeng, H. Zhong, Y. Luo, Q. Huang, X. Lin, and J. Liu, "Interfacial Engineering Principles for Hard Carbon Anodes in Sodium-Ion Batteries: From Mechanisms to Synergistic Strategies," *Energy & Environmental Science* 19 (2026): 1775, https://doi.org/10.1039/D5EE06849E.

224. J. P. Pender, G. Jha, D. H. Youn, et al., "Electrode Degradation in Lithium-Ion Batteries," *ACS Nano* 14 (2020): 1243–1295, https://doi.org/10.1021/acsnano.9b04365.

225. W. Li, C. Li, Y. Xu, et al., "Heteroatom-Doped and Graphitization-Enhanced Lignin-Derived Hierarchically Porous Carbon via Facile Assembly of Lignin-Fe Coordination for High-Voltage Symmetric Supercapacitors," *Journal of Colloid and Interface Science* 659 (2024): 374–384, https://doi.org/10.1016/j.jcis.2023.12.162.

226. O. Mašek, W. Buss, A. Roy-Poirier, et al., "Consistency of Biochar Properties over Time and Production Scales: A Characterisation of Standard Materials," *Journal of Analytical and Applied Pyrolysis* 132 (2018): 200–210, https://doi.org/10.1016/j.jaap.2018.02.020.

227. C.-H. Hsiao, S. Gupta, C.-Y. Lee, and N.-H. Tai, "Effects of Physical and Chemical Activations on the Performance of Biochar Applied in Supercapacitors," *Applied Surface Science* 610 (2023): 155560, https://doi.org/10.1016/j.apsusc.2022.155560.